fractal and fractional

MDPI

Article

Global Asymptotic Stability of a Fractional-Order Model for Mpox Dynamics with Media Effects

Ibraheem M. Alsulami [1,*] and Fahad Al Basir [2,*]

[1] Mathematics Department, Faculty of Science, Umm Al-Qura University, Makkah 21955, Saudi Arabia
[2] Department of Mathematics, Asansol Girls' College, Asansol 713304, India
* Correspondence: imsulami@uqu.edu.sa (I.M.A.); fahadalbasir@agc.ac.in or fahadbasir@gmail.com (F.A.B.)

Abstract

A fractional-order mathematical model is derived for mpox transmission dynamics that explicitly incorporates the influence of public awareness through a new awareness-dependent transmission function. The proposed incidence function models the reduction in disease transmission as the level of awareness increases, thereby capturing the dynamic interaction between epidemic progression and behavioral response. The model further accounts for asymptomatic infection, hospitalization, recovery, and awareness evolution using Caputo fractional derivatives to incorporate memory effects. Basic mathematical properties of the model, including positivity, boundedness, and existence of solutions, are established. The basic reproduction number, R_0, is derived using the next-generation matrix approach, and a sensitivity analysis is performed to identify the epidemiological parameters that most strongly influence disease transmission. Local and global stability analyses demonstrate that the disease-free equilibrium is locally and globally asymptotically stable whenever $R_0 < 1$, while an endemic equilibrium exists and is globally asymptotically stable when $R_0 > 1$ and a forward transcritical bifurcation occurs at $R_0 = 1$. Numerical simulations validate the analytical findings and illustrate the significant role of sustained public awareness in reducing disease transmission and mitigating epidemic outbreaks. The results obtained from the proposed model suggest that combining behavioral awareness strategies with conventional public health interventions can substantially improve the long-term control of mpox.

Keywords: fractional-order model; mpox transmission; awareness-dependent incidence; basic reproduction number (R_0); global stability; numerical simulation

Academic Editor: Corina S Drapaca

Received: 10 August 2026
Revised: 28 August 2026
Accepted: 29 August 2026
Published: 1 September 2026

1. Introduction

Mpox, which was formerly known as monkeypox, is a virus that has been receiving a lot of attention recently due to being a major health concern. It was once an endemic disease in Central and West Africa; however, it quickly expanded across continents in 2022. As a result, the World Health Organization declared it a Public Health Emergency of International Concern on 23 July 2022 [1,2]. The spread of the mpox virus occurs through close contact with the infected person, contaminated materials, and droplet infection. The significant point here is that both infected people and people who do not show any symptoms spread the virus [3].

Classic public health tools such as hospitalization, isolation of infected people, hospitalization, and contact tracing have been key factors for mpox containment [4,5]. However,

awareness campaigns in particular have become an equally important tool for mpox control and are mainly organized via media and social networks. Public awareness affects individual behavior by promoting preventive activities such as risk aversion, hygiene, visiting a doctor, and taking part in vaccinations [6–8]. Furthermore, campaigns increase the effectiveness of health measures by fighting false information and reducing stigma, thus improving the situation with case detection [9,10]. Such behavioral aspects make the inclusion of awareness into epidemic models necessary as they provide a more realistic model of epidemic processes.

Mathematical modeling is one of the core principles in the study of infectious diseases because of its importance in determining epidemic thresholds, trends of outbreaks, and intervention efficacy [11–13]. In the case of mpox, mathematical models have been used in the estimation of outbreaks' magnitude as well as the effects of vaccination and quarantine measures [5]. However, most of the classical epidemic models are based on integer-order differential equations, implying that the progress of the disease is influenced by the present status of the system. Fractional calculus offers an efficient mathematical tool to overcome this weakness. Through the use of non-local operators, fractional-order models incorporate the effect of memory, which enables previous states of the system to be considered when studying its current state [14–16].

In the context of infectious disease modeling, global stability analysis plays a pivotal role in establishing the ultimate fate of the system irrespective of initial conditions [17–19]. While local stability provides insights into behavior near equilibrium points, global stability ensures that trajectories across the entire phase space converge to either the disease-free or endemic equilibrium [20]. This distinction is critical for epidemic forecasting and public health policy, as it determines whether eradication strategies are feasible when $R_0 \leq 1$ or whether persistent infection is inevitable when $R_0 > 1$ [21]. By ruling out oscillations, multiple attractors, or chaotic dynamics, global stability analysis provides the mathematical rigor necessary for reliable predictions and effective resource allocation, thereby strengthening the link between theoretical epidemiology and practical disease control [22]. Motivated by these considerations, the present study investigates the global stability properties of a fractional-order mathematical model for mpox transmission.

Current mathematical models of mpox have included key epidemiological aspects like awareness, behavior change, contact heterogeneity, and data from actual outbreaks. The significance of vaccination alongside the influence of behavior change due to awareness in reducing mpox transmission was illustrated by Lin et al. [23], whereas the relevance of behavior and contact heterogeneity was shown by Zhang et al. [24] through surveillance data. Models incorporating time delay have also been constructed, taking into consideration the incubation period and fitted to actual mpox cases [25]. Nonetheless, most existing models involve the use of integer-order differential equations. Unlike these previous works, we introduce awareness into our model through a fractional-order model system.

The local asymptotic stability properties of the mpox transmission model formulated in the integer-order framework were investigated in [26]. Furthermore, local stability analysis of a fractional-order mpox model was conducted in [27]. However, to the best of our knowledge, the global stability and long-term dynamical behavior of the fractional-order system have not yet been analytically investigated. Therefore, the present study focuses on the global dynamics of the proposed fractional-order mpox model, with particular emphasis on establishing its global stability properties.

While existing mpox transmission models commonly assume a constant transmission rate, we incorporate the effect of public awareness through the awareness-dependent incidence modification

$$f(M) = 1 - \phi M,$$

where $M(t)$ denotes the level of public awareness and ϕ represents the effectiveness of awareness in reducing disease transmission. This formulation differs from the approach adopted by Ibraheem [27], in which awareness is incorporated through a saturated incidence term of the form $\frac{\beta SI}{1+\phi W}$, thereby accounting for diminishing returns in the effectiveness of awareness interventions in mpox control. The linear awareness-dependent formulation adopted in the present study offers analytical tractability and facilitates the derivation of explicit global stability conditions. In particular, we establish that the disease-free equilibrium is globally asymptotically stable when $R_0 < 1$, whereas the endemic equilibrium is globally asymptotically stable when $R_0 > 1$. In contrast, the saturated incidence formulation captures more realistic behavioral responses, including potential limitations in the effectiveness of awareness campaigns [28]; however, the resulting nonlinear structure may render analytical global stability analysis considerably more challenging. Thus, although both modeling frameworks emphasize the important role of public awareness in reducing mpox transmission, the present formulation prioritizes analytical tractability and the derivation of rigorous global stability criteria, whereas [27] places greater emphasis on saturating behavioral effects and the optimal control of disease transmission.

In light of all these factors, this paper aims to provide a new model of mpox transmission, which takes into account the dynamical effects of public awareness. We adopt a global stability analysis framework with an awareness-dependent incidence term of the form $(1-\phi M)\,\beta SI$, where awareness reduces transmission proportionally and directly. On the one hand, the proposed function is meant to take into account the decrease in effective contacts due to awareness. Moreover, awareness in this model is itself considered a dynamic parameter since it increases with the growth of symptomatic cases and hospitalizations and decreases over time because of no new cases.

The model is analyzed by means of a qualitative study. We prove some key mathematical properties of the model, such as positivity and boundedness of the solutions, to ensure that the model is biologically feasible. The basic reproduction number is determined via the next-generation matrix method, and sensitivity analysis is conducted to determine the most sensitive parameters in transmission. The stability analysis shows that the disease-free equilibrium is both locally and globally asymptotically stable if $R_0 < 1$, whereas there exists an endemic equilibrium which is globally stable if $R_0 > 1$. Simulations confirm the analytical findings and highlight the importance of constant awareness in the reduction in transmission and the containment of the outbreak.

The rest of this paper is structured as follows. In Section 2, the formulation of the mpox disease transmission model with an awareness-based incidence rate is provided. In Section 3, the mathematical analysis of the properties of the model, such as positivity, boundedness, existence, and uniqueness of solutions are analyzed. Existence of equilibria and the basic reproduction number are derived in Section 4. Local and global stability analyses of the equilibria are performed in Section 5. Numerical simulations are presented in Section 6, with a sensitivity analysis of model parameters. Finally, conclusions of the results are stated in Section 7.

2. Model Formulation

We construct a fractional-order SEIR-type model with additional compartments to capture both epidemiological and behavioral dynamics of disease transmission.

2.1. Fractional Derivative

Fractional calculus extends classical differentiation and integration to non-integer orders, enabling the modeling of systems with memory. To incorporate memory-dependent behavior into the proposed framework, we introduce the Caputo fractional derivative with

order $\alpha \in (0, 1]$. For a sufficiently differentiable function $f(t)$, this fractional derivative is given by

$$^{C}D_{t}^{\alpha} f(t) = \frac{1}{\Gamma(1-\alpha)} \int_{0}^{t} (t-\xi)^{-\alpha} f'(\xi)\, d\xi,$$

where $\Gamma(\cdot)$ denotes the Gamma function. Unlike the conventional integer-order derivative, the Caputo operator captures the contribution of the system's earlier states to its present behavior. Consequently, it is well-suited for representing memory-dependent and hereditary characteristics within the model.

2.2. Model Assumptions

The proposed model consists of seven compartments, namely, $S(t)$ for susceptible individuals, $E(t)$ for individuals who have been exposed but are not yet infectious, $A(t)$ for asymptomatic infectious individuals, $I(t)$ for symptomatic infectious individuals, $H(t)$ for hospitalized or isolated individuals, $R(t)$ for recovered individuals, and $M(t)$ for the level of awareness in the population. Interaction between the populations is presented in Figure 1.

The model integrates epidemiological progression with behavioral responses, while fractional derivatives provide flexibility in describing memory effects.

(H1) Susceptible individuals enter the population at a constant recruitment rate Λ, while natural mortality affects individuals in all compartments at the per-capita rate μ. The disease is transmitted through interactions with both symptomatic and asymptomatic infectious individuals, with corresponding transmission rates denoted by β_1 and β_2, respectively.

(H2) Awareness reduces transmission, with effective rates $(1 - \phi M)\beta_1$ and $(1 - \phi M)\beta_2$. Awareness is assumed to act only as a protective mechanism, never reducing transmission below zero.

(H3) Exposed individuals progress at a rate of θ, with fraction p becoming asymptomatic and $(1 - p)$ symptomatic and dying naturally at a rate of μ.

(H4) Asymptomatic infected individuals are assumed to recover at a rate γ_A. Symptomatic individuals may follow one of three possible paths: they can recover at a rate of γ_I, die from the disease at a rate of δ, or be moved to the hospitalized class at a rate of σ.

(H5) Hospitalized individuals either recover at a rate of γ_H or experience disease-induced death at a rate of δ_H. Once an individual recovers from the infection, they are assumed to remain immune and cannot be reinfected.

(H6) Changes in the level of awareness are associated with the total number of symptomatic and hospitalized individuals $(I + H)$. We assume η as proportionally constant. In particular, it can be defined as the frequency of awareness campaigns. Awareness gradually declines at a rate of ω when there are no new infection-related influences.

(H7) The epidemic dynamics are described using the Caputo fractional derivative of order $\alpha \in (0, 1]$. This fractional formulation allows the model to reflect the influence of previous states on the current evolution of the system.

(H8) We impose the parameter restriction

$$\phi \leq \frac{\omega\mu}{\eta\Lambda}, \tag{1}$$

which ensures that the quantity $1 - \phi M$ remains positive for all admissible values of the awareness variable M. Accordingly, the function

$$f(M) = 1 - \phi M$$

is considered to decrease strictly as the level of awareness M increases.

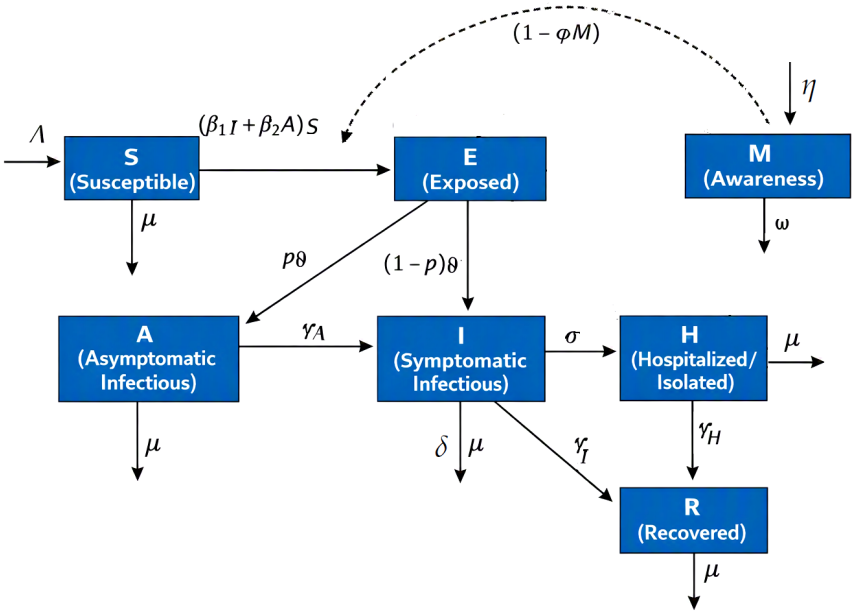

Figure 1. Schematic diagram of model (2).

2.3. Model Equations

From the above assumptions, we have the following system of equations for mpox dynamics:

$$\begin{aligned}
D_t^\alpha S &= \Lambda - \beta_1(1-\phi M)SI - \beta_2(1-\phi M)SA - \mu S,\\
D_t^\alpha E &= \beta_1(1-\phi M)SI + \beta_2(1-\phi M)SA - (\theta+\mu)E,\\
D_t^\alpha A &= p\theta E - (\gamma_A+\mu)A,\\
D_t^\alpha I &= (1-p)\theta E - (\gamma_I+\delta+\mu)I - \sigma I,\\
D_t^\alpha H &= \sigma I - (\gamma_H+\delta_H+\mu)H,\\
D_t^\alpha R &= \gamma_A A + \gamma_I I + \gamma_H H - \mu R,\\
D_t^\alpha M &= \eta(I+H) - \omega M.
\end{aligned} \tag{2}$$

The initial values of the populations are

$$\begin{aligned}
S(0) &= S_0 \geq 0, \quad E(0) = E_0 \geq 0, \quad A(0) = A_0 \geq 0,\\
I(0) &= I_0 \geq 0, \quad H(0) = H_0 \geq 0, \quad R(0) = R_0 \geq 0, \quad M(0) = M_0 \geq 0.
\end{aligned} \tag{3}$$

In this formulation, $S_0, E_0, A_0, I_0, H_0, R_0$, and M_0 represent the initial populations in the respective compartments, all assumed to be nonnegative to ensure biologically realistic initial conditions. Short description of the parameters and their baseline values are listed in Table 1.

Remark 1. *(i) The functional form* $(1-\phi M)$ *used to represent awareness impact is chosen for analytical convenience. An alternative nonlinear form could be considered for relevance to real-world behavioral data. The linear awareness function was adopted because of its simplicity, analytical tractability, and widespread use in epidemiological modeling studies.*

(ii) The condition $\phi\eta\Lambda \leq \omega\mu$ *is introduced to guarantee mathematical well-posedness and positivity of solutions. Figure 2 shows that* $f(M) = 1 - \phi M$ *is always positive and decreasing with* M *when* (1) *is considered.*

Table 1. Baseline parameter values and concise descriptions used in the model [8,23,27,29]. The natural mortality rate is taken as $\mu = 0.01, \text{day}^{-1}$. Though this value is higher than the natural mortality rate when interpreted on a literal daily time scale, this value is adopted as a model assumption to investigate the qualitative dynamical behavior of the proposed fractional-order system (2).

Parameter	Description	Value (Unit)
Λ	Recruitment rate of susceptible individuals	20 humans day^{-1}
β_1	Transmission rate due to symptomatic infection	0.002 $\text{human}^{-1}\text{day}^{-1}$
β_2	Transmission rate due to asymptomatic infection	0.0015 $\text{human}^{-1}\text{day}^{-1}$
θ	Progression rate from exposed to infectious class	0.2 day^{-1}
p	Proportion of exposed individuals becoming asymptomatic	0.3
γ_A	Recovery rate of asymptomatic individuals	0.10 day^{-1}
γ_I	Recovery rate of symptomatic individuals	0.08 day^{-1}
γ_H	Recovery rate of hospitalized individuals	0.07 day^{-1}
δ	Disease-induced mortality rate of symptomatic individuals	0.02 day^{-1}
δ_H	Disease-induced mortality rate of hospitalized individuals	0.01 day^{-1}
σ	Hospitalization (or isolation) rate	0.05 day^{-1}
μ	Natural mortality rate	0.01 day^{-1}
ϕ	Effectiveness coefficient of awareness	0.04
η	Awareness growth rate driven by infection cases	0.0001 human^{-1} day^{-1}
ω	Awareness decay rate	0.015 day^{-1}

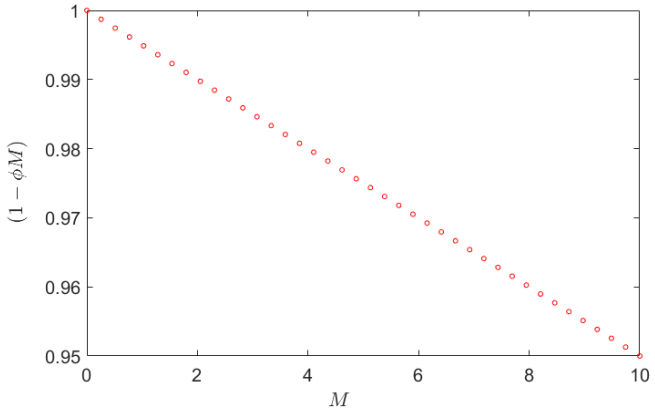

Figure 2. Plot of the awareness function $(1 - \phi M)$ with M under the restriction (1).

3. Existence, Nonnegativity, and Boundedness of Solutions

We now examine the solvability of system (2) subject to the prescribed initial conditions (3). The following theorem establishes the well-posedness of the problem. In epidemiological modeling, it is also essential to verify that the trajectories of the system remain biologically admissible. Specifically, all compartments must be nonnegative and bounded for every $t \geq 0$. Therefore, we derive the following theorem.

Theorem 1. *Suppose that hypotheses* $(H1)$–$(H8)$ *are satisfied. Then, for every finite horizon* $T > 0$, *system* (2) *admits a unique trajectory* $(S(t), E(t), A(t), I(t), H(t), R(t), M(t))$, $t \in [0, T]$. *Moreover, for every nonnegative initial condition satisfying* (3), *the solution remains nonnegative and bounded for all* $t \geq 0$. *In particular, letting* $Y(t) = S(t) + E(t) + A(t) + I(t) + H(t) + R(t)$, *the region*

$$\Omega = \left\{ (S, E, A, I, H, R, M) \in \mathbb{R}^7_+ : Y(t) \leq K_Y,\ M(t) \leq K_M \right\}, \tag{4}$$

where $K_Y = \max\left\{Y_0, \frac{\Lambda}{\mu}\right\}$, $K_M = \max\left\{M_0, \frac{\eta K_Y}{\omega}\right\}$, *is positively invariant, and every solution of system* (2) *with nonnegative initial data remains confined to* Ω *for all* $t \geq 0$.

Proof. Let us define $X(t) = \big(S(t), E(t), A(t), I(t), H(t), R(t), M(t)\big)^T$ and $F = (F_1, F_2, F_3, F_4, F_4, F_5, F_6, F_7)^T$, where $F_i, i = 1, 2, \ldots, 7$ are the right sides of (2). Then, system (2) can be written in the compact form

$$^{C}D_t^{\alpha} X(t) = F(X(t)),\ X(0) = X_0, \tag{5}$$

where $0 < \alpha \leq 1$, and $X_0 = (S_0, E_0, A_0, I_0, H_0, R_0, M_0)^T$. Each component of F is a polynomial in the state variables. Thus, every component of F is continuously differentiable with respect to the state variables; we have $F \in C^1(\mathbb{R}^7, \mathbb{R}^7)$; and its Jacobian matrix $DF(Y)$ is continuous on $\mathbb{R}^7$. Let, $\Omega \subset \mathbb{R}^7$ be any bounded convex subset of the feasible region. Since DF is continuous, it is bounded on Ω; that is, there exists a constant $L_\Omega > 0$ such that

$$\sup_{Y \in \Omega} \|DF(Y)\| \leq L_\Omega.$$

For any $Y, Z \in \Omega$, the line segment joining Y and Z lies in Ω. Therefore, by the integral form of the mean-value theorem,

$$F(Y) - F(Z) = \int_0^1 DF\big(Z + \tau(Y - Z)\big)(Y - Z)\, d\tau.$$

Taking norms, we obtain

$$\|F(Y) - F(Z)\| \leq \int_0^1 \big\|DF\big(Z + \tau(Y - Z)\big)\big\| \|Y - Z\|\, d\tau \quad \leq L_\Omega \|Y - Z\|.$$

Hence, F satisfies local Lipschitz continuity in the feasible region. Therefore, by the standard existence and uniqueness theorem for Caputo fractional differential equations [30], system (2) admits a unique local solution on a maximal interval $[0, T_{\max})$, where $0 < T_{\max} \leq \infty$.

We now establish the positivity and boundedness of the solutions. In particular, we show that the nonnegative orthant is positively invariant under hypotheses $(H1)$–$(H8)$. Indeed, when a component reaches zero, the corresponding right-hand side is nonnegative. We check that

$$\begin{aligned}
&F_1(X)|_{S=0} = \Lambda \geq 0, \quad F_2(X)|_{E=0} = \beta_1(1 - \phi M)SI + \beta_2(1 - \phi M)SA \geq 0,\\
&F_3(X)|_{A=0} = p\theta E \geq 0, \quad F_4(X)|_{I=0} = (1 - p)\theta E \geq 0, F_5(X)|_{H=0} = \sigma I \geq 0,\\
&F_6(X)|_{R=0} = \gamma_A A + \gamma_I I + \gamma_H H \geq 0, \text{ and } F_7(X)|_{M=0} = \eta(I + H) \geq 0.
\end{aligned}$$

Thus, the vector field points inward on every boundary hyperplane of $\mathbb{R}+^7$. Therefore, by the generalized positivity theorem for Caputo fractional differential systems, trajectories initiating in $\mathbb{R}+^7$ cannot leave the nonnegative region. Hence, we conclude that for nonnegative initial conditions, all components of the solution remain nonnegative.

Now, define the total population $Y(t) = S(t) + E(t) + A(t) + I(t) + H(t) + R(t)$. Then, adding the first six equations of system (2), we can obtain

$$^{C}D_t^{\alpha} Y(t) = \Lambda - \mu Y(t) - \delta I(t) - \delta_H H(t) \leq \Lambda - \mu Y(t). \tag{6}$$

By the comparison principle for Caputo fractional differential equations,

$$Y(t) \leq Y_0 E_\alpha(-\mu t^\alpha) + \frac{\Lambda}{\mu}[1 - E_\alpha(-\mu t^\alpha)],$$

where $Y_0 = S_0 + E_0 + A_0 + I_0 + H_0 + R_0$ and $E_\alpha(\cdot)$ denotes the Mittag–Leffler function. Consequently,

$$Y(t) \leq K_Y, \qquad K_Y := \max\left\{Y_0, \frac{\Lambda}{\mu}\right\}, \quad t \geq 0.$$

Thus, $0 \leq S(t), E(t), A(t), I(t), H(t), R(t) \leq K_Y$. It remains to show the boundedness of $M(t)$. From the last equation of system (2), we have

$${}^{C}D_t^{\alpha} M(t) = \eta(I + H) - \omega M.$$

Since $I(t), H(t) \leq K_Y$, we can write

$${}^{C}D_t^{\alpha} M(t) \leq \eta K_Y - \omega M(t).$$

Another application of the fractional comparison principle yields

$$M(t) \leq M_0 E_\alpha(-\omega t^\alpha) + \frac{\eta K_Y}{\omega}[1 - E_\alpha(-\omega t^\alpha)].$$

This gives

$$0 \leq M(t) \leq K_M, \quad K_M := \max\left\{M_0, \frac{\eta K_Y}{\omega}\right\}.$$

Therefore, all components of $Y(t)$ remain nonnegative and bounded on every finite time interval.

Finally, suppose, for contradiction, that $T_{\max} < \infty$. The above a prior estimates imply that

$$\sup_{0 \leq t < T_{\max}} \|Y(t)\| < \infty.$$

Thus, the solution remains in a bounded subset of the feasible region as $t \to T_{\max}$. Since F is locally Lipschitz on this region, the local existence and uniqueness theorem can be applied at $T_{\max}$ to extend the solution beyond $T_{\max}$. This contradicts the maximality of $T_{\max}$. Therefore, $T_{\max} = \infty$.

Hence, system (2) admits a unique nonnegative global solution for every nonnegative initial condition (3). In particular, for every finite horizon $T > 0$, system (2) possesses a unique trajectory $(S(t), E(t), A(t), I(t), H(t), R(t), M(t))$, $t \in [0, T]$. □

Remark 2. *From the boundedness result, $M(t) \leq \frac{\eta\Lambda}{\omega\mu}$. Assumption $(H8)$ gives*

$$\phi \leq \frac{\omega\mu}{\eta\Lambda}, \tag{7}$$

This implies that $\phi M(t) \leq 1$, and therefore, $1 - \phi M(t) \geq 0$ for all $t \geq 0$. Consequently, the awareness-modified transmission terms remain nonnegative throughout the feasible region, ensuring the biological consistency of the model.

4. Model Analysis

In this section, we determine the equilibria of system (2), derive the basic reproduction number, and perform a stability analysis of equilibria.

4.1. Equilibria

The dynamical system admits two distinct equilibria, namely

(i) the disease-free equilibrium (DFE), $\mathcal{E}_0 = \left(\frac{\Lambda}{\mu}, 0, 0, 0, 0, 0, 0, 0\right)$. This configuration corresponds to the absence of infection in the population, with only susceptible individuals present.

(ii) the endemic equilibrium, $\mathcal{E}^* = (S^*, E^*, A^*, I^*, H^*, R^*, M^*)$, where each component represents the steady-state values of the respective compartments in the presence of persistent infection. Here,

$$\begin{aligned} E^* &= \frac{\omega}{\eta c_I(1+c_H)}M^*, \\ I^* &= c_I E^* = \frac{\omega}{\eta(1+c_H)}M^*, \\ A^* &= c_A E^* = \frac{c_A}{c_I}I^*, \\ H^* &= c_H I^*, \\ S^* &= \frac{\theta+\mu}{(1-\phi M^*)(\beta_1 c_I+\beta_2 c_A)}, \\ R^* &= \frac{1}{\mu}(\gamma_A A^* + \gamma_I I^* + \gamma_H H^*). \end{aligned}$$

The equilibrium value M^* satisfies

$$g(M) = -K_2\phi M^2 + (K_2 + K_3\phi)M + (K_1 - K_3) = 0, \tag{8}$$

where

$$K_1 = (\theta+\mu)(v+\mu), K_2 = (\theta+\mu)\frac{\omega}{\eta(1+c_H)}\left(\beta_1 + \beta_2\frac{c_A}{c_I}\right), K_3 = \Lambda(\beta_1 c_I + \beta_2 c_A),$$

with

$$c_A = \frac{p\theta}{\gamma_A+\mu},\ c_I = \frac{(1-p)\theta}{\gamma_I+\delta+\mu+\sigma}, c_H = \frac{\sigma}{\gamma_H+\delta_H+\mu}.$$

4.2. The Basic Reproduction Number

The basic reproduction number, denoted by R_0, is derived using the next-generation matrix method. This quantity represents the expected number of secondary infections generated by a typical infectious individual introduced into a completely susceptible population.

For the construction of the next-generation matrix, we consider the infected-state system with variable $x = (E, A, I)^T$. Among these variables, new infections enter only the exposed class. Hence, the vector containing the rates of appearance of new infections can be written as

$$\mathcal{F}(x) = \begin{bmatrix} \beta_1 SI + \beta_2 SA \\ 0 \\ 0 \end{bmatrix}.$$

The remaining transfers between the infected compartments are collected in the vector

$$\mathcal{V}(x) = \begin{bmatrix} (\theta+\mu)E \\ (\gamma_A+\mu)A - p\theta E \\ (\gamma_I+\delta+\mu+\sigma)I - (1-p)\theta E \end{bmatrix}.$$

At the disease-free equilibrium, the susceptible population is denoted by $\bar{S}$, while $E = A = I = 0$. Taking the Jacobian matrices of $\mathcal{F}(x)$ and $\mathcal{V}(x)$ with respect to (E, A, I) and evaluating them at the DFE gives

$$F = \begin{bmatrix} 0 & \beta_2\bar{S} & \beta_1\bar{S} \\ 0 & 0 & 0 \\ 0 & 0 & 0 \end{bmatrix},$$

and

$$V = \begin{bmatrix} \theta + \mu & 0 & 0 \\ -p\theta & \gamma_A + \mu & 0 \\ -(1-p)\theta & 0 & \gamma_I + \delta + \mu + \sigma \end{bmatrix}.$$

The next-generation matrix is consequently defined by

$$K = FV^{-1}.$$

According to the next-generation matrix approach, the basic reproduction number is given by the spectral radius of K. After evaluating the spectral radius and simplifying, we obtain

$$R_0 = \frac{\bar{S}}{\theta + \mu}\left[\frac{p\theta\beta_2}{\gamma_A + \mu} + \frac{(1-p)\theta\beta_1}{\gamma_I + \delta + \mu + \sigma}\right]. \tag{9}$$

The two terms in the brackets correspond to the contributions from the asymptomatic and symptomatic transmission pathways, respectively. The first term represents the contribution of asymptomatic infectious individuals, whereas the second term accounts for transmission generated by symptomatic individuals.

Using the disease-free susceptible population $\bar{S} = \frac{\Lambda}{\mu}$, the basic reproduction number takes the following explicit form:

$$R_0 = \frac{\Lambda}{\mu(\theta + \mu)}\left[\frac{p\theta\beta_2}{\gamma_A + \mu} + \frac{(1-p)\theta\beta_1}{\gamma_I + \delta + \mu + \sigma}\right]. \tag{10}$$

We use this expression as a threshold value to study the stability of DFE and the existence of bifurcation.

5. Stability Analysis

We now examine the local and global stability properties of the equilibria. The discussion begins with the disease-free equilibrium (DFE).

5.1. Local Stability of the DFE

The Jacobian matrix evaluated at $\mathcal{E}_0$ takes the form

$$J(\mathcal{E}_0) = [J_{ij}]_{7\times 7} = \begin{bmatrix} -\mu & 0 & 0 & -\beta_1\bar{S} & 0 & 0 & 0 \\ 0 & -(\theta+\mu) & \beta_2\bar{S} & \beta_1\bar{S} & 0 & 0 & 0 \\ 0 & p\theta & -(\gamma_A+\mu) & 0 & 0 & 0 & 0 \\ 0 & (1-p)\theta & 0 & J_{44} & 0 & 0 & 0 \\ 0 & 0 & 0 & \sigma & J_{55} & 0 & 0 \\ 0 & 0 & \gamma_A & \gamma_I & \gamma_H & -\mu & 0 \\ 0 & 0 & 0 & \eta & \eta & 0 & -\omega \end{bmatrix},$$

where

$$J_{44} = -(\gamma_I + \sigma + \mu + \delta), \qquad J_{55} = -(\gamma_H + \delta_H + \mu).$$

For convenience, let $l_1 = \gamma_I + \sigma + \mu + \delta = -J_{44}$, $l_2 = \gamma_H + \delta_H + \mu = -J_{55}$. The following four eigenvalues are obtained from the block-triangular structure of $J(\mathcal{E}_0)$:

$$\rho_1 = -\mu,\ \rho_2 = -l_2,\ \rho_3 = -\mu, \text{ and } \rho_4 = -\omega,$$

We note that these four eigenvalues are strictly negative. The remaining three eigenvalues are determined by the following equation:

$$h(\rho) = \rho^3 + a_1\rho^2 + a_2\rho + a_3 = 0, \tag{11}$$

where

$$a_1 = \theta + \gamma_A + 2\mu + l_1,\ a_2 = (\theta+\mu)(\gamma_A+\mu) + l_1(\theta+\gamma_A+2\mu) - p\theta\beta_2\bar{S} - (1-p)\theta\beta_1\bar{S},$$

and

$$a_3 = l_1(\theta+\mu)(\gamma_A+\mu) - p\theta\beta_2\bar{S}l_1 - (1-p)\theta\beta_1\bar{S}(\gamma_A+\mu).$$

Using the expression of the basic reproduction number R_0 in (10), the constant coefficient of the characteristic polynomial can be written as

$$a_3 = (\theta+\mu)(\gamma_A+\mu)l_1(1-R_0). \tag{12}$$

To verify the remaining Routh–Hurwitz condition, let

$$l_3 = \theta+\mu,\ l_4 = \gamma_A+\mu,\ l_5 = p\theta\beta_2\bar{S},\ l_6 = (1-p)\theta\beta_1\bar{S}.$$

Then

$$R_0 = \frac{l_5}{l_3 l_4} + \frac{l_6}{l_1 l_3}.$$

Hence, if $R_0 < 1$,

$$l_5 l_1 + l_6 l_4 < l_1 l_3 l_4. \tag{13}$$

The coefficients of the characteristic polynomial can be written as

$$a_1 = l_3 + l_4 + l_1,\ a_2 = l_3 l_4 + l_1(l_3+l_4) - l_5 - l_6, \text{ and } a_3 = l_1 l_3 l_4 - l_5 l_1 - l_6 l_4.$$

Therefore,

$$a_1 a_2 - a_3 = (l_3+l_4)l_3 l_4 + l_1(l_3+l_4)(l_3+l_4+l_1) - l_5(l_3+l_4) - l_6(l_3+l_1).$$

Since $l_5, l_6 > 0$ and (13) holds, we have $l_5 < l_3 l_4,\ l_6 < l_1 l_3$. Thus,

$$l_5(l_3+l_4) + l_6(l_3+l_1) < l_3 l_4(l_3+l_4) + l_1 l_3(l_3+l_1).$$

Moreover,

$$l_3 l_4(l_3+l_4) + l_1 l_3(l_3+l_1) < l_3 l_4(l_3+l_4) + l_1(l_3+l_4)(l_3+l_4+l_1),$$

since

$$l_1(l_3+l_4)(l_3+l_4+l_1) - l_1 l_3(l_3+l_1) = l_1\left[l_4(l_3+l_1) + (l_3+l_4)^2\right] > 0.$$

Thus, we conclude that

$$a_1 a_2 - a_3 > 0.$$

Hence, for $R_0 < 1$, the Routh–Hurwitz condition $a_1 a_2 > a_3$ is satisfied.

For a fractional-order dynamical system with order $\alpha \in (0, 1]$, the local asymptotic stability of the DFE ($\mathcal{E}_0$) is determined by the location of the eigenvalues of the Jacobian matrix $J(E_0)$ in the complex plane. According to the Matignon stability criterion, $\mathcal{E}_0$ is locally asymptotically stable if and only if every eigenvalue ρ of $J(\mathcal{E}_0)$ satisfies

$$|\arg(\rho)| > \frac{\alpha\pi}{2}. \tag{14}$$

To establish this condition, we first apply the classical Routh–Hurwitz criterion to the cubic polynomial (11). All three roots have negative real parts if

$$a_1 > 0,\ a_2 > 0,\ a_3 > 0,\ a_1 a_2 > a_3.$$

When $R_0 < 1$, it follows that $a_3 = (\theta + \mu)(\gamma_A + \mu) l_1 (1 - R_0) > 0$.

Thus, Routh–Hurwitz inequalities are satisfied. Therefore, all three roots of (11) have negative real parts. Together with the five negative eigenvalues, we have $\mathrm{Re}(\rho) < 0$ for every eigenvalue ρ of $J(\mathcal{E}_0)$. Consequently,

$$|\arg(\rho)| > \frac{\pi}{2} \geq \frac{\alpha\pi}{2}, \quad 0 < \alpha \leq 1,$$

and hence, the Matignon stability condition (14) is satisfied.

Now, for $R_0 > 1$, we have

$$a_3 = (\theta + \mu)(\gamma_A + \mu) l_1 (1 - R_0) < 0.$$

Also, since $h(0) = a_3 < 0$ and $\lim_{\rho \to +\infty} h(\rho) = +\infty$, the cubic polynomial (11) possesses at least one positive real root. Hence, $J(E_0)$ has an eigenvalue $\rho > 0$. For this eigenvalue, $|\arg(\rho)| = 0 < \frac{\alpha\pi}{2}$, so the Matignon stability condition is violated. Therefore, $\mathcal{E}_0$ is unstable.

From the above discussion, we have the following theorem.

Theorem 2. *The disease-free equilibrium $\mathcal{E}_0$ is locally asymptotically stable when $R_0 < 1$ and unstable when $R_0 > 1$.*

Remark 3. *The above analysis gives a clear link between the characteristic polynomial, Routh–Hurwitz criteria, the basic reproduction number, and the Matignon stability condition. The general fractional Routh–Hurwitz theorem presented earlier in this subsection becomes redundant since it is not needed for our present result. In this case, the discussion of the discriminant of the characteristic polynomial and the different cases of α become unnecessary since we deal with the model in which $0 < \alpha \leq 1$ and $R_0 < 1$, and therefore, $\mathrm{Re}(\rho) < 0$ for all eigenvalues.*

5.2. Global Stability of the Disease-Free Equilibrium (DFE)

We now investigate the global stability of the disease-free equilibrium (DFE) of system (2).

Theorem 3. *The disease-free equilibrium $\mathcal{E}_0$ is globally asymptotically stable in Ω.*

Proof. Consider the Lyapunov function

$$V(E, A, I) = c_1 E + c_2 A + c_3 I, \tag{15}$$

where $c_1, c_2, c_3 > 0$ are constants to be determined. Taking the Caputo fractional derivative of V along the trajectories of system (2), we obtain

$$\begin{aligned} D_t^\alpha V &= c_1 D_t^\alpha E + c_2 D_t^\alpha A + c_3 D_t^\alpha I \\ &= c_1 \Big[(1 - \phi M) S(\beta_1 I + \beta_2 A) - (\theta + \mu) E \Big] \\ &\quad + c_2 \Big[p\theta E - (\gamma_A + \mu) A \Big] + c_3 \Big[(1 - p)\theta E - (\gamma_I + \delta + \sigma + \mu) I \Big]. \end{aligned}$$

Using the boundedness of solutions, we can write

$$\begin{aligned} D_t^\alpha V \leq c_1 \left[\frac{\Lambda\beta_2}{\mu} A + \frac{\Lambda\beta_1}{\mu} I - (\theta+\mu)E \right] \\ + c_2[p\theta E - (\gamma_A+\mu)A] \\ + c_3[(1-p)\theta E - (\gamma_I+\delta+\sigma+\mu)I]. \end{aligned}$$

We choose

$$c_2 = \frac{c_1\Lambda\beta_2}{\mu(\gamma_A+\mu)} \text{ and } c_3 = \frac{c_1\Lambda\beta_1}{\mu(\gamma_I+\delta+\sigma+\mu)}.$$

Then, the A- and I-terms cancel, and hence, we have

$$D_t^\alpha V \leq -c_1(\theta+\mu)E + \frac{c_1\Lambda\beta_2 p\theta}{\mu(\gamma_A+\mu)}E + \frac{c_1\Lambda\beta_1(1-p)\theta}{\mu(\gamma_I+\delta+\sigma+\mu)}E.$$

Using the consistently defined reproduction number in (10), we obtain

$$\begin{aligned} D_t^\alpha V &\leq -c_1(\theta+\mu)\left[1 - \frac{\Lambda\theta}{\mu(\theta+\mu)}\left(\frac{p\beta_2}{\gamma_A+\mu} + \frac{(1-p)\beta_1}{\gamma_I+\delta+\sigma+\mu}\right)\right]E \\ &= -c_1(\theta+\mu)(1-\mathcal{R}_0)E. \end{aligned}$$

Therefore, whenever $\mathcal{R}_0 < 1$, we have $D_t^\alpha V \leq 0$. Also, $D_t^\alpha V = 0$ when $E = 0$.

Now, we determine the largest invariant subset of

$$\mathcal{Z} = \{(S, E, A, I, H, R, M) \in \Omega : D_t^\alpha V = 0\}.$$

Since $\mathcal{R}_0 < 1$, it follows that

$$\mathcal{Z} \subseteq \{E = 0\}.$$

Thus, the largest invariant subset contained in $\mathcal{Z}$ is the singleton $\mathcal{E}_0 = \left(\frac{\Lambda}{\mu}, 0, 0, 0, 0, 0, 0\right)$.

By the fractional LaSalle invariance principle, every solution of system (2) that starts in Ω approaches this largest invariant subset as $t \to \infty$. Therefore,

$$\lim_{t\to\infty}(S, E, A, I, H, R, M) = \left(\frac{\Lambda}{\mu}, 0, 0, 0, 0, 0, 0\right).$$

Hence, the disease-free equilibrium $\mathcal{E}_0$ is globally asymptotically stable whenever $\mathcal{R}_0 < 1$.

This completes the proof. □

5.3. Forward Bifurcation

In this case, the bifurcation analysis of the system in the vicinity of the critical value $R_0 = 1$ is presented. This analysis is performed based on the results obtained within the framework of the center manifold theory proposed by Castillo-Chavez and Song [31].

Let the coefficient of symptomatic infection β_1 be chosen as the bifurcation parameter. Then, denote by β_1^* the critical value of β_1 such that the condition $R_0 = 1$ is satisfied. At $\beta = \beta^*$, the Jacobian matrix at the point $\mathcal{E}_0$ has exactly one simple eigenvalue equal to zero. All other eigenvalues are located strictly in the left half-plane of the complex plane. So, the linearized system has a one-dimensional center subspace that allows us to apply the center manifold theorem to examine the bifurcation occurring at $R_0 = 1$.

Theorem 4. *Model system* (2) *undergoes a forward transcritical bifurcation at* $R_0 = 1$.

Proof. Let $X = (S, E, A, I, H, R, M)^T$, and rewrite system (2) as

$$D_t^\alpha X = F(X, \beta_1). \tag{16}$$

Taking β_1 as the bifurcation parameter, the Jacobian $J = D_X F(\mathcal{E}_0, \beta_1^*)$ has one simple zero eigenvalue at $R_0 = 1$.

Let $w = (w_1, \ldots, w_7)^T$ and $v = (v_1, \ldots, v_7)$ be the corresponding right and left eigenvectors associated with the zero eigenvalue, normalized so that

$$v \cdot w = 1.$$

According to the center manifold theorem of Castillo-Chavez and Song [31], we define the following coefficients:

$$a = \sum_{k,i,j} v_k w_i w_j \frac{\partial^2 F_k}{\partial x_i \partial x_j}(\mathcal{E}_0, \beta_1^*), \tag{17}$$

and

$$b = \sum_{k,i} v_k w_i \frac{\partial^2 F_k}{\partial x_i \partial \beta_1}(\mathcal{E}_0, \beta_1^*). \tag{18}$$

For convenience, let us define

$$d_A = \gamma_A + \mu, \qquad d_I = \gamma_I + \sigma + \mu + \delta, \qquad d_H = \gamma_H + \delta_H + \mu, \qquad \bar{S} = \frac{\Lambda}{\mu}.$$

We first determine the right eigenvector explicitly. At $\beta_1 = \beta_1^*$, the right eigenvector w satisfies

$$J(\mathcal{E}_0) w = 0. \tag{19}$$

Choosing $w_2 = 1$, the third, fourth, fifth, and seventh rows of $J(\mathcal{E}_0)w = 0$ yield

$$p\theta w_2 - d_A w_3 = 0,$$

$$(1-p)\theta w_2 - d_I w_4 = 0,$$

$$\sigma w_4 - d_H w_5 = 0,$$

and

$$\eta w_4 + \eta w_5 - \omega w_7 = 0.$$

Consequently,

$$w_3 = \frac{p\theta}{d_A}, \qquad w_4 = \frac{(1-p)\theta}{d_I}, \qquad w_5 = \frac{\sigma(1-p)\theta}{d_I d_H},$$

and

$$w_7 = \frac{\eta}{\omega}(w_4 + w_5) = \frac{\eta(1-p)\theta}{\omega d_I}\left(1 + \frac{\sigma}{d_H}\right).$$

The first row yields

$$-\mu w_1 - \beta_1^* \bar{S} w_4 = 0,$$

and hence,

$$w_1 = -\frac{\beta_1^* \bar{S}}{\mu} w_4 = -\frac{\beta_1^*(1-p)\theta\bar{S}}{\mu d_I}.$$

Finally, from the sixth row, we get

$$\gamma_A w_3 + \gamma_I w_4 + \gamma_H w_5 - \mu w_6 = 0,$$

so that

$$w_6 = \frac{1}{\mu}\left[\frac{\gamma_A p\theta}{d_A} + \frac{\gamma_I(1-p)\theta}{d_I} + \frac{\gamma_H\sigma(1-p)\theta}{d_I d_H}\right].$$

Therefore, a convenient choice of the right eigenvector is

$$w = \begin{pmatrix} -\frac{\beta_1^*(1-p)\theta\bar{S}}{\mu d_I} \\ 1 \\ \frac{p\theta}{d_A} \\ \frac{(1-p)\theta}{d_I} \\ \frac{\sigma(1-p)\theta}{d_I d_H} \\ \frac{1}{\mu}\left[\frac{\gamma_A p\theta}{d_A} + \frac{\gamma_I(1-p)\theta}{d_I} + \frac{\gamma_H\sigma(1-p)\theta}{d_I d_H}\right] \\ \frac{\eta(1-p)\theta}{\omega d_I}\left(1+\frac{\sigma}{d_H}\right) \end{pmatrix}.$$

Thus, $w_1 < 0$, whereas $w_2, w_3, w_4, w_5, w_6, w_7 > 0$ for biologically feasible parameter values.

We solve the following equation to get the left eigenvector

$$vJ(\mathcal{E}_0) = 0.$$

From the first, fifth, sixth, and seventh columns, we have

$$v_1 = v_5 = v_6 = v_7 = 0.$$

The third column gives

$$\beta_2\bar{S}v_2 - d_A v_3 = 0,$$

and therefore,

$$v_3 = \frac{\beta_2\bar{S}}{d_A}v_2.$$

The second column gives

$$-(\theta+\mu)v_2 + p\theta v_3 + (1-p)\theta v_4 = 0,$$

which yields

$$v_4 = \frac{(\theta+\mu) - p\theta\beta_2\bar{S}/d_A}{(1-p)\theta}v_2.$$

Taking $v_2 = 1$ before normalization, we obtain

$$\widetilde{v} = \begin{pmatrix} 0 \\ 1 \\ \frac{\beta_2\bar{S}}{d_A} \\ \frac{(\theta+\mu) - p\theta\beta_2\bar{S}/d_A}{(1-p)\theta} \\ 0 \\ 0 \\ 0 \end{pmatrix}.$$

To impose the normalization $v \cdot w = 1$, we define

$$D = \widetilde{v} \cdot w.$$

Since only the second, third, and fourth components of $\widetilde{v}$ are nonzero,

$$D = w_2 + \frac{\beta_2 \bar{S}}{d_A} w_3 + \frac{(\theta + \mu) - p\theta\beta_2 \bar{S}/d_A}{(1-p)\theta} w_4.$$

Using $w_2 = 1$, $w_3 = p\theta/d_A$, and $w_4 = (1-p)\theta/d_I$, we obtain

$$D = 1 + \frac{p\theta\beta_2 \bar{S}}{d_A^2} + \frac{(\theta + \mu) - p\theta\beta_2 \bar{S}/d_A}{d_I}.$$

Thus, the normalized left eigenvector satisfying $v \cdot w = 1$ is given by

$$v = \frac{1}{D} \begin{pmatrix} 0 \\ 1 \\ \dfrac{\beta_2 \bar{S}}{d_A} \\ \dfrac{(\theta + \mu) - p\theta\beta_2 \bar{S}/d_A}{(1-p)\theta} \\ 0 \\ 0 \\ 0 \end{pmatrix}.$$

At the critical value $R_0 = 1$, the fourth-column equation of $vJ = 0$ is satisfied because

$$\beta_1^* \bar{S} = d_I v_4 / v_2,$$

which is equivalent to the threshold relation obtained from the second row of $Jw = 0$.

The only nonlinear terms in the present model arising from the incidence functions are $(1 - \phi M)\beta_1 SI$, and $(1 - \phi M)\beta_2 SA$. Since $S = \frac{\Lambda}{\mu}$ at the disease-free equilibrium and $M = 0$, the second-order partial derivatives satisfy

$$\frac{\partial^2 F}{\partial S \partial I} > 0, \quad \frac{\partial^2 F}{\partial S \partial A} > 0,$$

while the term generated by $(1 - \phi M)$ introduces negative nonlinear feedback through

$$\frac{\partial^2 F}{\partial M \partial I} < 0, \quad \frac{\partial^2 F}{\partial M \partial A} < 0.$$

More explicitly, because the nonlinear incidence terms occur in the susceptible and exposed equations with opposite signs, and because $v_1 = 0$, only the second component F_2 contributes to the coefficient a. The nonzero second-order partial derivatives of F_2 that contribute to a are

$$\left.\frac{\partial^2 F_2}{\partial S \partial I}\right|_{\mathcal{E}_0} = \beta_1^*, \qquad \left.\frac{\partial^2 F_2}{\partial S \partial A}\right|_{\mathcal{E}_0} = \beta_2,$$

and

$$\left.\frac{\partial^2 F_2}{\partial M \partial I}\right|_{\mathcal{E}_0} = -\phi\beta_1^* \bar{S}, \qquad \left.\frac{\partial^2 F_2}{\partial M \partial A}\right|_{\mathcal{E}_0} = -\phi\beta_2 \bar{S}.$$

By symmetry of the mixed second-order derivatives, the corresponding derivatives with the variables interchanged have the same values. Hence, the four pairs (S, I), (S, A), (M, I), and (M, A) each occur twice in the double sum defining a. Therefore,

$$\begin{aligned} a = {} & 2v_2\beta_1^* w_1 w_4 + 2v_2\beta_2 w_1 w_3 \\ & - 2v_2\phi\beta_1^*\bar{S} w_4 w_7 - 2v_2\phi\beta_2\bar{S} w_3 w_7. \end{aligned}$$

Substituting $v_2 = 1/D$ and the expressions for the components of w, the first contribution is

$$\begin{aligned} 2v_2\beta_1^* w_1 w_4 &= \frac{2}{D}\beta_1^*\left(-\frac{\beta_1^*(1-p)\theta\bar{S}}{\mu d_I}\right)\left(\frac{(1-p)\theta}{d_I}\right) \\ &= -\frac{2}{D}\frac{(\beta_1^*)^2(1-p)^2\theta^2\bar{S}}{\mu d_I^2}. \end{aligned}$$

Similarly, the second contribution is

$$\begin{aligned} 2v_2\beta_2 w_1 w_3 &= \frac{2}{D}\beta_2\left(-\frac{\beta_1^*(1-p)\theta\bar{S}}{\mu d_I}\right)\left(\frac{p\theta}{d_A}\right) \\ &= -\frac{2}{D}\frac{\beta_1^*\beta_2 p(1-p)\theta^2\bar{S}}{\mu d_A d_I}. \end{aligned}$$

For the third contribution, we have

$$\begin{aligned} -2v_2\phi\beta_1^*\bar{S} w_4 w_7 = {} & -\frac{2}{D}\phi\beta_1^*\bar{S}\left(\frac{(1-p)\theta}{d_I}\right)\left[\frac{\eta(1-p)\theta}{\omega d_I}\left(1+\frac{\sigma}{d_H}\right)\right] \\ = {} & -\frac{2}{D}\frac{\phi\beta_1^*\eta(1-p)^2\theta^2\bar{S}}{\omega d_I^2}\left(1+\frac{\sigma}{d_H}\right). \end{aligned}$$

Finally, the fourth contribution is

$$\begin{aligned} -2v_2\phi\beta_2\bar{S} w_3 w_7 = {} & -\frac{2}{D}\phi\beta_2\bar{S}\left(\frac{p\theta}{d_A}\right)\left[\frac{\eta(1-p)\theta}{\omega d_I}\left(1+\frac{\sigma}{d_H}\right)\right] \\ = {} & -\frac{2}{D}\frac{\phi\beta_2 p\eta(1-p)\theta^2\bar{S}}{\omega d_A d_I}\left(1+\frac{\sigma}{d_H}\right). \end{aligned}$$

Combining the above four contributions gives

$$\begin{aligned} a = -\frac{2}{D}\Bigg[& \frac{(\beta_1^*)^2(1-p)^2\theta^2\bar{S}}{\mu d_I^2} + \frac{\beta_1^*\beta_2 p(1-p)\theta^2\bar{S}}{\mu d_A d_I} \\ & + \frac{\phi\beta_1^*\eta(1-p)^2\theta^2\bar{S}}{\omega d_I^2}\left(1+\frac{\sigma}{d_H}\right) \\ & + \frac{\phi\beta_2 p\eta(1-p)\theta^2\bar{S}}{\omega d_A d_I}\left(1+\frac{\sigma}{d_H}\right)\Bigg]. \end{aligned}$$

All parameters appearing in the square brackets are positive for biologically feasible parameter values, with $0 < p < 1$ and $D > 0$. Therefore, every term inside the square brackets is positive, which immediately proves $a < 0$.

For b, the bifurcation parameter β_1 occurs only in the incidence term $(1-\phi M)\beta_1 SI$. At $\mathcal{E}_0$,

$$\left.\frac{\partial^2 F_2}{\partial I\,\partial\beta_1}\right|_{\mathcal{E}_0} = \bar{S}, \qquad \left.\frac{\partial^2 F_2}{\partial S\,\partial\beta_1}\right|_{\mathcal{E}_0} = I_0 = 0,$$

and the derivatives involving M vanish at $\mathcal{E}_0$. Since $v_1 = 0$, the contribution from the susceptible equation is zero. Consequently,

$$b = v_2 w_4 \bar{S}.$$

Using $v_2 = \frac{1}{D}$, $w_4 = \frac{(1-p)\theta}{d_I}$, and $\bar{S} = \frac{\Lambda}{\mu}$, we obtain

$$b = \frac{1}{D}\frac{(1-p)\theta}{d_I}\frac{\Lambda}{\mu} > 0.$$

This implies that $a < 0$ and $b > 0$. Hence, $a \neq 0$ and $b \neq 0$, and the non-degeneracy conditions required for the application of the Castillo-Chavez–Song criterion are fulfilled. It follows from Theorem 4.1 of Castillo-Chavez and Song [31] that the model exhibits a forward transcritical bifurcation at $R_0 = 1$.

This completes the proof. □

5.4. Local Stability of the Endemic Equilibrium (EE)

To investigate the stability of the endemic equilibrium, we focus on the infection-related compartments (E, A, I, H, M). Accordingly, the Jacobian matrix is restricted to this subsystem and takes the form

$$J = [a_{ij}]_{7\times 7} = \begin{bmatrix} a_{11} & 0 & -\beta_2(1-\phi M)S & -\beta_1(1-\phi M)S & 0 & 0 & a_{17} \\ a_{21} & -(\theta+\mu) & \beta_2(1-\phi M)S & \beta_1(1-\phi M)S & 0 & 0 & a_{27} \\ 0 & p\theta & -(\gamma_A+\mu) & 0 & 0 & 0 & 0 \\ 0 & (1-p)\theta & 0 & -a_{45} & 0 & 0 & 0 \\ 0 & 0 & 0 & \sigma & a_{55} & 0 & 0 \\ 0 & 0 & \gamma_A & \gamma_I & \gamma_H & -\mu & 0 \\ 0 & 0 & 0 & \eta & \eta & 0 & -\omega \end{bmatrix},$$

where

$$\begin{aligned} a_{11} &= -\beta_1(1-\phi M)I - \beta_2(1-\phi M)A - v - \mu, \\ a_{21} &= \beta_1(1-\phi M)I + \beta_2(1-\phi M)A, \\ a_{55} &= J_{55}, \\ a_{17} &= \phi(\beta_1 SI + \beta_2 SA), \\ a_{27} &= -\phi(\beta_1 SI + \beta_2 SA), \\ a_{45} &= \gamma_I + \delta + \mu + \sigma. \end{aligned}$$

The characteristic polynomial of the Jacobian is

$$\chi(\rho) = (\rho+\mu)^2(\rho - a_{55})(\rho+\omega)\,P(\rho),$$

with

$$P(\rho) = \rho^4 + b_1\rho^3 + b_2\rho^2 + b_3\rho + b_4,$$

where the coefficients are given by

$$\begin{aligned} a_1 &= -a_{11} + (\theta+\mu) + (\gamma_A+\mu) + a_{45}, \\ a_2 &= (\theta+\mu)(\gamma_A+\mu) - (\theta+\mu)a_{45} - (\gamma_A+\mu)a_{45} \\ &\quad + a_{11}\big((\theta+\mu) + (\gamma_A+\mu) + a_{45}\big) \\ &\quad - a_{21}\,\beta_2(1-\phi M)S - p\theta\,\beta_2(1-\phi M)S - (1-p)\theta\,\beta_1(1-\phi M)S, \end{aligned}$$

$$
\begin{aligned}
a_3 = &-a_{11}\Big((\theta+\mu)(\gamma_A+\mu)+(\theta+\mu)a_{45}+(\gamma_A+\mu)a_{45}\Big)\\
&+(\theta+\mu)(\gamma_A+\mu)a_{45}-a_{21}\Big(p\theta a_{45}+(1-p)\theta(\gamma_A+\mu)\Big)\\
&-a_{17}\Big(p\theta\beta_1(1-\phi M)S+(1-p)\theta\beta_2(1-\phi M)S\Big)\\
&-a_{27}\Big(p\theta\beta_1(1-\phi M)S+(1-p)\theta\beta_2(1-\phi M)S\Big),\\
a_4 = &\,a_{11}(\theta+\mu)(\gamma_A+\mu)a_{45}\\
&-a_{21}\Big(p\theta a_{45}\,\beta_2(1-\phi M)S+(1-p)\theta(\gamma_A+\mu)\,\beta_1(1-\phi M)S\Big)\\
&+a_{17}\Big(p\theta\beta_1(1-\phi M)Sa_{45}+(1-p)\theta\beta_2(1-\phi M)S(\gamma_A+\mu)\Big)\\
&+a_{27}\Big(p\theta\beta_1(1-\phi M)Sa_{45}+(1-p)\theta\beta_2(1-\phi M)S(\gamma_A+\mu)\Big).
\end{aligned}
$$

For the fractional-order system governed by a Caputo derivative of order $\alpha \in (0,1]$, the endemic equilibrium $\mathcal{E}^*$ is locally asymptotically stable precisely when all eigenvalues ρ_i of the Jacobian matrix satisfy

$$|\arg(\rho_i)| > \frac{\alpha\pi}{2}, \qquad i = 1,\ldots,5. \tag{20}$$

In other words, condition (20) requires every eigenvalue of the Jacobian to remain outside the sector centered on the positive real axis with opening angle $\alpha\pi$.

Let $D(P)$ denote the discriminant of the quartic polynomial $P(\rho)$.

Proposition 1. *For $\alpha \in [0,2)$, if $D(P) < 0$, then the eigenvalues of the Jacobian satisfy condition (20) provided that*

$$a_3 > 0, \quad \tan^{-1}\left(\frac{-3\sqrt{3}(y-\nu)}{3(y+\nu)+2a_1}\right) > \frac{\alpha\pi}{2},$$

where

$$y = \sqrt[3]{-\tfrac{n}{2}+\sqrt{\tfrac{m^3}{27}+\tfrac{n^2}{4}}}, \quad \nu = \sqrt[3]{-\tfrac{n}{2}-\sqrt{\tfrac{m^3}{27}+\tfrac{n^2}{4}}},$$

with

$$m = b_2 - \frac{b_1^2}{3}, \quad n = \frac{2b_1^3}{27} - \frac{b_1 b_2}{3} + b_3.$$

Proof. We establish the global asymptotic stability of $\mathcal{E}^*$ by means of a Lyapunov function and the fractional LaSalle invariance principle. The main point is to retain all mixed terms generated by the nonlinear incidence function and the awareness dynamics and to explicitly show that they can be dominated by the negative quadratic terms.

Let $\mathcal{E}^* = (S^*, E^*, A^*, I^*, H^*, R^*, M^*)$ denote the endemic equilibrium of system (2). The equilibrium coordinates satisfy

$$\Lambda = (1-\phi M^*)S^*(\beta_1 I^* + \beta_2 A^*) + \mu S^*, \tag{21}$$
$$(1-\phi M^*)S^*(\beta_1 I^* + \beta_2 A^*) = (\theta+\mu)E^*, \tag{22}$$
$$p\theta E^* = (\gamma_A+\mu)A^*, \tag{23}$$
$$(1-p)\theta E^* = (\gamma_I+\delta+\mu+\sigma)I^*, \tag{24}$$
$$\sigma I^* = (\gamma_H+\delta_H+\mu)H^*, \tag{25}$$
$$\gamma_A A^* + \gamma_I I^* + \gamma_H H^* = \mu R^*, \tag{26}$$
$$\eta(I^*+H^*) = \omega M^*. \tag{27}$$

We consider the following Lyapunov function

$$\begin{aligned}\mathcal{L} = \quad & c_1\left(S - S^* - S^* \ln \tfrac{S}{S^*}\right) + c_2\left(E - E^* - E^* \ln \tfrac{E}{E^*}\right) \\ & + c_3\left(A - A^* - A^* \ln \tfrac{A}{A^*}\right) + c_4\left(I - I^* - I^* \ln \tfrac{I}{I^*}\right) \\ & + c_5\left(H - H^* - H^* \ln \tfrac{H}{H^*}\right) + c_6\left(M - M^* - M^* \ln \tfrac{M}{M^*}\right).\end{aligned} \tag{28}$$

where $c_i > 0$, $i = 1, \ldots, 6$. Now, for $x > 0$, the function

$$x - x^* - x^* \ln \frac{x}{x^*}$$

is nonnegative and vanishes if and only if $x = x^*$. Using this, we have

$$\mathcal{L} \geq 0,$$

with equality if and only if $S = S^*, E = E^*, A = A^*, I = I^*, H = H^*, M = M^*$. Thus, $\mathcal{L}$ is positive definite with respect to the endemic equilibrium in the variables appearing in (28).

For $0 < \alpha \leq 1$, the standard inequality for the Caputo derivative gives

$$D_t^\alpha\left(x - x^* - x^* \ln \frac{x}{x^*}\right) \leq \left(1 - \frac{x^*}{x}\right) D_t^\alpha x.$$

Consequently,

$$\begin{aligned}D_t^\alpha \mathcal{L} \leq \quad & c_1\left(1 - \tfrac{S^*}{S}\right) D_t^\alpha S + c_2\left(1 - \tfrac{E^*}{E}\right) D_t^\alpha E \\ & + c_3\left(1 - \tfrac{A^*}{A}\right) D_t^\alpha A + c_4\left(1 - \tfrac{I^*}{I}\right) D_t^\alpha I \\ & + c_5\left(1 - \tfrac{H^*}{H}\right) D_t^\alpha H + c_6\left(1 - \tfrac{M^*}{M}\right) D_t^\alpha M.\end{aligned} \tag{29}$$

Now, we define the function

$$G(S, I, A, M) = (1 - \phi M) S(\beta_1 I + \beta_2 A),$$

and thus,

$$G^* = (1 - \phi M^*) S^* (\beta_1 I^* + \beta_2 A^*).$$

From the endemic equilibrium relations (21) and (22), we have

$$G^* = (\theta + \mu) E^*, \qquad \Lambda = G^* + \mu S^*.$$

Substituting the model equations into (29) and using the equilibrium relations, we obtain

$$\begin{aligned}D_t^\alpha \mathcal{L} \leq \quad & -c_1 \mu \tfrac{(S - S^*)^2}{S} - c_2(\theta + \mu) \tfrac{(E - E^*)^2}{E} \\ & - c_3(\gamma_A + \mu) \tfrac{(A - A^*)^2}{A} - c_4(\gamma_I + \delta + \mu + \sigma) \tfrac{(I - I^*)^2}{I} \\ & - c_5(\gamma_H + \delta_H + \mu) \tfrac{(H - H^*)^2}{H} - c_6 \omega \tfrac{(M - M^*)^2}{M} + \mathcal{Q},\end{aligned} \tag{30}$$

where $\mathcal{Q}$ denotes the collection of all mixed terms.

We now estimate these mixed terms explicitly.

First, we consider the S–E contribution

$$\mathcal{Q}_{SE} = \left[c_2\left(1 - \frac{E^*}{E}\right) - c_1\left(1 - \frac{S^*}{S}\right)\right](G - G^*). \tag{31}$$

To make the structure of this term explicit, introduce the deviations

$$\Delta S = S - S^*, \qquad \Delta E = E - E^*, \qquad \Delta A = A - A^*, \qquad \Delta I = I - I^*, \qquad \Delta M = M - M^*.$$

Then

$$1-\frac{E^*}{E}=\frac{E-E^*}{E}=\frac{\Delta E}{E},\qquad 1-\frac{S^*}{S}=\frac{S-S^*}{S}=\frac{\Delta S}{S}.$$

Hence, (31) can be rewritten as

$$\begin{aligned}\mathcal{Q}_{SE} &= \left(c_2\tfrac{\Delta E}{E}-c_1\tfrac{\Delta S}{S}\right)(G-G^*)\\ &= c_2\tfrac{\Delta E}{E}(G-G^*)-c_1\tfrac{\Delta S}{S}(G-G^*).\end{aligned} \tag{32}$$

The difference $G-G^*$ can be decomposed as

$$\begin{aligned}G-G^* = \quad & (1-\phi M)S[\beta_1(I-I^*)+\beta_2(A-A^*)]\\ & +(1-\phi M)(S-S^*)(\beta_1 I^*+\beta_2 A^*)\\ & -\phi(M-M^*)S^*(\beta_1 I^*+\beta_2 A^*)\\ & -\phi(M-M^*)(S-S^*)(\beta_1 I^*+\beta_2 A^*).\end{aligned} \tag{33}$$

For clarity, the above identity follows by first adding and subtracting $(1-\phi M)S(\beta_1 I^*+\beta_2 A^*)$:

$$\begin{aligned}G-G^* = \quad & (1-\phi M)S[(\beta_1 I+\beta_2 A)-(\beta_1 I^*+\beta_2 A^*)]\\ & +[(1-\phi M)S-(1-\phi M^*)S^*](\beta_1 I^*+\beta_2 A^*).\end{aligned} \tag{34}$$

Moreover,

$$\begin{aligned}&(1-\phi M)S-(1-\phi M^*)S^*\\ &\quad=(1-\phi M)(S-S^*)-\phi(M-M^*)S^*-\phi(M-M^*)(S-S^*).\end{aligned} \tag{35}$$

Substituting (35) into (34) gives (33).

Therefore, the dependence of the incidence function on awareness is retained explicitly, including all terms involving $M-M^*$.

By assumption $(H8)$, $\phi\le\frac{\omega\mu}{\eta\Lambda}$, and since $M(t)\le\frac{\eta\Lambda}{\omega\mu}$ in Ω, it follows that $0<1-\phi M(t)\le 1$. Consequently, the coefficients appearing in the incidence terms are bounded on Ω.

Using (32) and (33), the incidence contribution consists of terms of the generic forms $\frac{\Delta E}{E}\Delta I$, $\frac{\Delta E}{E}\Delta A$, $\frac{\Delta E}{E}\Delta S$, $\frac{\Delta E}{E}\Delta M$, together with $\frac{\Delta S}{S}\Delta I$, $\frac{\Delta S}{S}\Delta A$, $\frac{\Delta S}{S}\Delta S$, $\frac{\Delta S}{S}\Delta M$. For example, for bounded coefficients $K_{EI},K_{EA}>0$, Young's inequality gives

$$K_{EI}\left|\frac{\Delta E}{E}\Delta I\right|\le\frac{\varepsilon_{EI}}{2}\frac{\Delta E^2}{E}+\frac{K_{EI}^2}{2\varepsilon_{EI}}\frac{E}{1}\Delta I^2, \tag{36}$$

$$K_{EA}\left|\frac{\Delta E}{E}\Delta A\right|\le\frac{\varepsilon_{EA}}{2}\frac{\Delta E^2}{E}+\frac{K_{EA}^2}{2\varepsilon_{EA}}\frac{E}{1}\Delta A^2. \tag{37}$$

Since Ω is bounded, the remaining state-dependent coefficients can be absorbed into finite constants. Thus, after collecting all incidence-generated terms, there exist nonnegative constants $\kappa_{SE}^{(S)},\kappa_{SE}^{(E)},\kappa_{SE}^{(A)},\kappa_{SE}^{(I)},\kappa_{SE}^{(M)}$ such that

$$\begin{aligned}\mathcal{Q}_{SE}\le \quad & \kappa_{SE}^{(S)}\tfrac{(S-S^*)^2}{S}+\kappa_{SE}^{(E)}\tfrac{(E-E^*)^2}{E}\\ & +\kappa_{SE}^{(A)}\tfrac{(A-A^*)^2}{A}+\kappa_{SE}^{(I)}\tfrac{(I-I^*)^2}{I}+\kappa_{SE}^{(M)}\tfrac{(M-M^*)^2}{M}.\end{aligned} \tag{38}$$

For the awareness equation, using $\eta(I^*+H^*)=\omega M^*$, we obtain

$$\mathcal{Q}_M=c_6\eta\frac{M-M^*}{M}[(I-I^*)+(H-H^*)]. \tag{39}$$

Writing the two cross terms separately,

$$\mathcal{Q}_M = c_6\eta\frac{M-M^*}{M}(I-I^*) + c_6\eta\frac{M-M^*}{M}(H-H^*). \tag{40}$$

For the first term, Young's inequality yields

$$c_6\eta\left|\frac{M-M^*}{M}(I-I^*)\right| \le \frac{c_6\eta\varepsilon_1}{2}\frac{(M-M^*)^2}{M} + \frac{c_6\eta}{2\varepsilon_1}\frac{(I-I^*)^2}{M}, \tag{41}$$

while for the second term,

$$c_6\eta\left|\frac{M-M^*}{M}(H-H^*)\right| \le \frac{c_6\eta\varepsilon_2}{2}\frac{(M-M^*)^2}{M} + \frac{c_6\eta}{2\varepsilon_2}\frac{(H-H^*)^2}{M}. \tag{42}$$

Adding these two inequalities gives

$$\begin{aligned}\mathcal{Q}_M \le\ & \tfrac{c_6\eta}{2}(\varepsilon_1+\varepsilon_2)\tfrac{(M-M^*)^2}{M} \\ & + \tfrac{c_6\eta}{2\varepsilon_1}\tfrac{(I-I^*)^2}{M} + \tfrac{c_6\eta}{2\varepsilon_2}\tfrac{(H-H^*)^2}{M}.\end{aligned} \tag{43}$$

The mixed terms generated by the A, I, and H equations are

$$\mathcal{Q}_A = c_3p\theta\left(1-\frac{A^*}{A}\right)(E-E^*), \tag{44}$$

$$\mathcal{Q}_I = c_4(1-p)\theta\left(1-\frac{I^*}{I}\right)(E-E^*), \tag{45}$$

$$\mathcal{Q}_H = c_5\sigma\left(1-\frac{H^*}{H}\right)(I-I^*). \tag{46}$$

Since

$$1-\frac{A^*}{A} = \frac{A-A^*}{A},\ 1-\frac{I^*}{I} = \frac{I-I^*}{I},\ 1-\frac{H^*}{H} = \frac{H-H^*}{H},$$

we can write

$$\mathcal{Q}_A = c_3p\theta\frac{A-A^*}{A}(E-E^*), \tag{47}$$

$$\mathcal{Q}_I = c_4(1-p)\theta\frac{I-I^*}{I}(E-E^*), \tag{48}$$

$$\mathcal{Q}_H = c_5\sigma\frac{H-H^*}{H}(I-I^*). \tag{49}$$

Thus, each of these terms is a product of two deviations and can be controlled by Young's inequality.

For arbitrary $\rho_A, \rho_I, \rho_H > 0$, Young's inequality gives

$$|\mathcal{Q}_A| \le \frac{\rho_A}{2}\frac{(E-E^*)^2}{E} + \frac{c_3^2p^2\theta^2}{2\rho_A}\frac{E(A^*)^2}{A^2}, \tag{50}$$

$$|\mathcal{Q}_I| \le \frac{\rho_I}{2}\frac{(E-E^*)^2}{E} + \frac{c_4^2(1-p)^2\theta^2}{2\rho_I}\frac{E(I^*)^2}{I^2}, \tag{51}$$

$$|\mathcal{Q}_H| \le \frac{\rho_H}{2}\frac{(I-I^*)^2}{I} + \frac{c_5^2\sigma^2}{2\rho_H}\frac{I(H^*)^2}{H^2}. \tag{52}$$

On the bounded positively invariant region Ω, the remaining state-dependent coefficients in (50)–(52) can be bounded above by finite constants. Therefore, these estimates can be written in the quadratic form

$$|\mathcal{Q}_A| \le \widehat{\kappa}_A^{(E)} \frac{(E-E^*)^2}{E} + \widehat{\kappa}_A^{(A)} \frac{(A-A^*)^2}{A}, \tag{53}$$

$$|\mathcal{Q}_I| \le \widehat{\kappa}_I^{(E)} \frac{(E-E^*)^2}{E} + \widehat{\kappa}_I^{(I)} \frac{(I-I^*)^2}{I}, \tag{54}$$

$$|\mathcal{Q}_H| \le \widehat{\kappa}_H^{(I)} \frac{(I-I^*)^2}{I} + \widehat{\kappa}_H^{(H)} \frac{(H-H^*)^2}{H}, \tag{55}$$

where all $\widehat{\kappa}$'s are nonnegative and finite.

More generally, after applying Young's inequality to every mixed term arising from (33), (43), and (44)–(46), all cross terms can be bounded in the form

$$\begin{aligned} \mathcal{Q} \le & \widetilde{\kappa}_1 \frac{(S-S^*)^2}{S} + \widetilde{\kappa}_2 \frac{(E-E^*)^2}{E} + \widetilde{\kappa}_3 \frac{(A-A^*)^2}{A} \\ & + \widetilde{\kappa}_4 \frac{(I-I^*)^2}{I} + \widetilde{\kappa}_5 \frac{(H-H^*)^2}{H} + \widetilde{\kappa}_6 \frac{(M-M^*)^2}{M}, \end{aligned} \tag{56}$$

where $\widetilde{\kappa}_i \ge 0$ denote the total contributions of the mixed terms associated with the ith state variable.

In particular, the constants $\widetilde{\kappa}_i$ collect the contributions from the separate estimates above; schematically,

$$\begin{aligned} \widetilde{\kappa}_1 &= \kappa_{SE}^{(S)} + \kappa_M^{(S)}, \\ \widetilde{\kappa}_2 &= \kappa_{SE}^{(E)} + \kappa_A^{(E)} + \kappa_I^{(E)}, \\ \widetilde{\kappa}_3 &= \kappa_{SE}^{(A)} + \kappa_A^{(A)}, \\ \widetilde{\kappa}_4 &= \kappa_{SE}^{(I)} + \kappa_M^{(I)} + \kappa_I^{(I)} + \kappa_H^{(I)}, \\ \widetilde{\kappa}_5 &= \kappa_M^{(H)} + \kappa_H^{(H)}, \\ \widetilde{\kappa}_6 &= \kappa_{SE}^{(M)} + \kappa_M^{(M)}. \end{aligned} \tag{57}$$

The exact values depend on the selected Young parameters and the bounds of the coefficients on Ω.

We now choose the positive constants c_i and the Young parameters so that

$$\begin{aligned} c_1\mu &> \widetilde{\kappa}_1, & c_2(\theta+\mu) &> \widetilde{\kappa}_2, \\ c_3(\gamma_A+\mu) &> \widetilde{\kappa}_3, & c_4(\gamma_I+\delta+\mu+\sigma) &> \widetilde{\kappa}_4, \\ c_5(\gamma_H+\delta_H+\mu) &> \widetilde{\kappa}_5, & c_6\omega &> \widetilde{\kappa}_6. \end{aligned} \tag{58}$$

Under these conditions, define

$$\begin{aligned} \kappa_1 &= c_1\mu - \widetilde{\kappa}_1 > 0, & \kappa_2 &= c_2(\theta+\mu) - \widetilde{\kappa}_2 > 0, \\ \kappa_3 &= c_3(\gamma_A+\mu) - \widetilde{\kappa}_3 > 0, & \kappa_4 &= c_4(\gamma_I+\delta+\mu+\sigma) - \widetilde{\kappa}_4 > 0, \\ \kappa_5 &= c_5(\gamma_H+\delta_H+\mu) - \widetilde{\kappa}_5 > 0, & \kappa_6 &= c_6\omega - \widetilde{\kappa}_6 > 0. \end{aligned} \tag{59}$$

Substituting (56) into (30), we obtain

$$\begin{aligned} D_t^\alpha \mathcal{L} \le & -(c_1\mu - \widetilde{\kappa}_1)\tfrac{(S-S^*)^2}{S} \\ & -(c_2(\theta+\mu) - \widetilde{\kappa}_2)\tfrac{(E-E^*)^2}{E} \\ & -(c_3(\gamma_A+\mu) - \widetilde{\kappa}_3)\tfrac{(A-A^*)^2}{A} \\ & -(c_4(\gamma_I+\delta+\mu+\sigma) - \widetilde{\kappa}_4)\tfrac{(I-I^*)^2}{I} \\ & -(c_5(\gamma_H+\delta_H+\mu) - \widetilde{\kappa}_5)\tfrac{(H-H^*)^2}{H} \\ & -(c_6\omega - \widetilde{\kappa}_6)\tfrac{(M-M^*)^2}{M}. \end{aligned} \tag{60}$$

Using the definitions of κ_i, Equation (60) becomes

$$D_t^\alpha \mathcal{L} \leq \begin{aligned} &-\kappa_1 \frac{(S-S^*)^2}{S} - \kappa_2 \frac{(E-E^*)^2}{E} - \kappa_3 \frac{(A-A^*)^2}{A} \\ &-\kappa_4 \frac{(I-I^*)^2}{I} - \kappa_5 \frac{(H-H^*)^2}{H} - \kappa_6 \frac{(M-M^*)^2}{M}. \end{aligned} \tag{61}$$

Since $S, E, A, I, H, M > 0$ in the interior of Ω and $\kappa_i > 0$, every term on the right-hand side is nonpositive. Furthermore,

$$D_t^\alpha \mathcal{L} = 0 \implies \begin{aligned} &\kappa_1 \frac{(S-S^*)^2}{S} + \kappa_2 \frac{(E-E^*)^2}{E} + \kappa_3 \frac{(A-A^*)^2}{A} \\ &+\kappa_4 \frac{(I-I^*)^2}{I} + \kappa_5 \frac{(H-H^*)^2}{H} + \kappa_6 \frac{(M-M^*)^2}{M} = 0. \end{aligned} \tag{62}$$

Because every summand is nonnegative and every κ_i is strictly positive, the sum can vanish only when

$$S = S^*, \quad E = E^*, \quad A = A^*, \quad I = I^*, \quad H = H^*, \quad M = M^*.$$

Thus, the derivative is negative definite with respect to the six variables included in the Lyapunov function.

It remains to determine the corresponding value of R. When

$$S = S^*, \quad E = E^*, \quad A = A^*, \quad I = I^*, \quad H = H^*, \quad M = M^*,$$

the R-equation becomes

$${}^C D_t^\alpha R = \gamma_A A^* + \gamma_I I^* + \gamma_H H^* - \mu R.$$

Using the equilibrium relation (26), $\gamma_A A^* + \gamma_I I^* + \gamma_H H^* = \mu R^*$, and hence ${}^C D_t^\alpha R = \mu(R^* - R)$. Consequently, the only invariant value of R is $R = R^*$. Thus, the largest invariant subset of

$$\{(S, E, A, I, H, R, M) \in \Omega : D_t^\alpha \mathcal{L} = 0\}$$

is the singleton $\{\mathcal{E}^*\}$. Therefore, by the fractional LaSalle invariance principle, every solution of system (2) with an initial condition in Ω approaches $\mathcal{E}^*$ as $t \to \infty$. Hence,

$$\lim_{t\to\infty} (S, E, A, I, H, R, M) = (S^*, E^*, A^*, I^*, H^*, R^*, M^*).$$

Therefore, the endemic equilibrium $\mathcal{E}^*$ is globally asymptotically stable in Ω.

This completes the proof. □

6. Numerical Simulations

This section provides the numerical verification of the analytical findings derived in the earlier sections. The parameter values used in this section are summarized in Table 1. The numerical experiments have been carried out over a time period of 1000–1200 days with the parameter values as shown in Table 1. The natural mortality rate being constant at $\mu = 0.01$ day^{-1}, the trajectories show the effect of natural mortality as well as that of the disease-related dynamics for the assumed set of parameter values. The relatively large value of μ is considered for long-term simulation results.

The fractional-order epidemic model is solved numerically by employing the *fractional Adams–Bashforth–Moulton (ABM) predictor–corrector scheme* for the Caputo fractional derivative of order α, where $0 < \alpha \leq 1$. To this end, the system is first reformulated in its

equivalent Volterra integral form and discretized on a uniform temporal grid $t_n = nh$, with h denoting the step size.

At each time step, the *fractional Adams–Bashforth formula* is applied to generate a predicted solution. Subsequently, the *Adams–Moulton formula* is utilized to obtain the corrected solution. The nonlinear terms are evaluated at the predicted and corrected states, respectively. This predictor–corrector procedure is iterated over the entire computational interval, thereby yielding numerical approximations of the state variables $\big(S(t), E(t), A(t), I(t), H(t), R(t), M(t)\big)$. It is noteworthy that the method naturally incorporates the *memory effect* associated with the fractional derivative, since the evaluation at each time step depends on the complete history of the solution at all preceding time nodes.

This section presents numerical simulations that illustrate and validate the analytical results obtained in the preceding sections. Model (2) is solved using the fractional Adams–Bashforth–Moulton predictor–corrector scheme [32]. Parameter values are taken from Table 1, and the simulations are carried out accordingly to demonstrate the dynamical behavior of the system under fractional-order derivatives.

Solution trajectories of the system (2) with parameters that fulfill the condition $R_0 < 1$ are depicted in Figure 3a–g. It can be observed that the system tends to the equilibrium state without the disease, which is labeled by E_0. The outcome is achieved due to low infection rates as well as increased treatment rates, making the disease eradicated. Therefore, the system can achieve a disease-free equilibrium state in some cases by choosing appropriate parameters. The values of eigenvalues have been determined as $-0.0100, -0.0600, -0.0100, -0.0150, -0.0900, -0.3238, -0.0367$, and -0.1196. It is clear that the condition $|\arg(\rho)| > \frac{\alpha\pi}{2}$ holds true for each eigenvalue ρ.

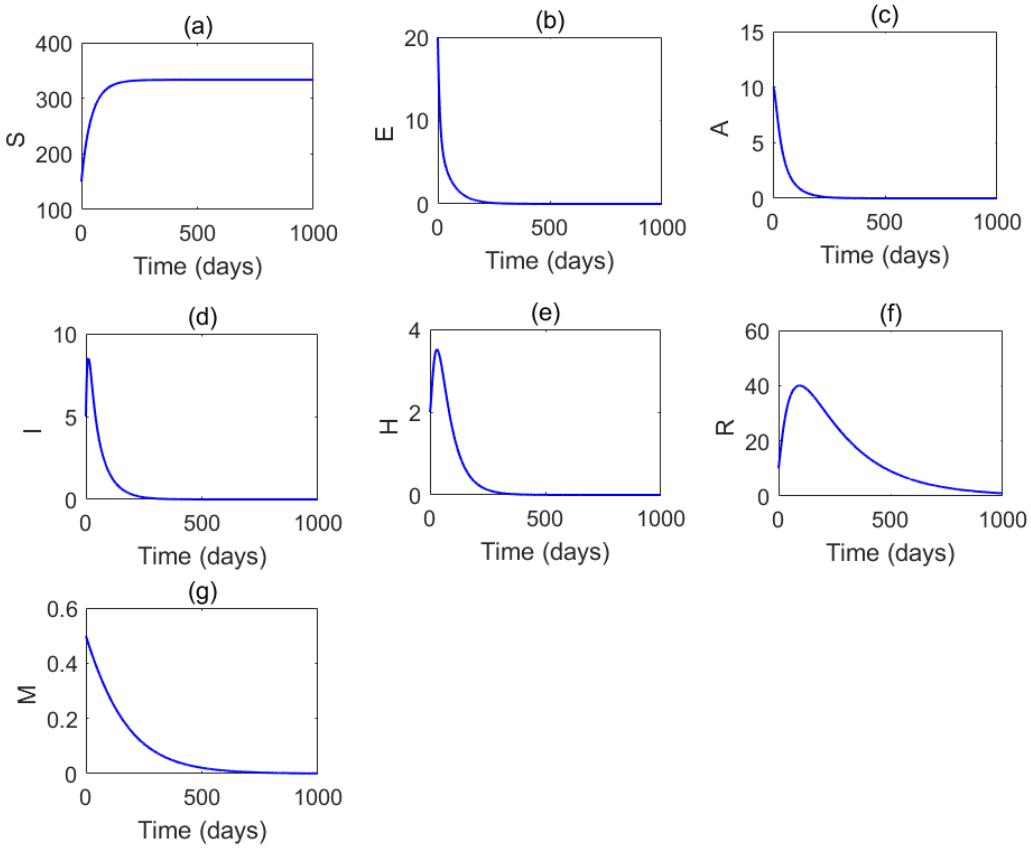

Figure 3. (**a**–**g**) Time series solutions are plotted for $R_0 < 1$. Parameters values are taken from Table 1 except $\beta_1 = 0.00025$.

Stability regions of the disease-free equilibrium (DFE) for the mpox transmission model are shown in Figure 4. Right panel illustrates the β_1–β_2 plane, where β_1 denotes the transmission rate from symptomatic individuals and β_2 denotes the transmission rate from asymptomatic individuals. The shaded region corresponds to parameter combinations yielding $R_0 < 1$, ensuring local stability of the DFE, while the boundary contour line marks the critical boundary $R_0 = 1$. Left panel depicts the β_1–θ plane, with θ representing the progression rate from exposed to infectious individuals. Again, shaded domains indicate stability ($R_0 < 1$), and the boundary line delineates the threshold of instability. This figure demonstrates that increases in transmission or progression rates reduce the stability region, thereby favoring endemic persistence. The awareness condition $\phi \leq \frac{\omega\mu}{\eta\Lambda}$ is satisfied under the chosen parameter set, confirming that the shaded regions represent feasible stability domains for the mpox DFE.

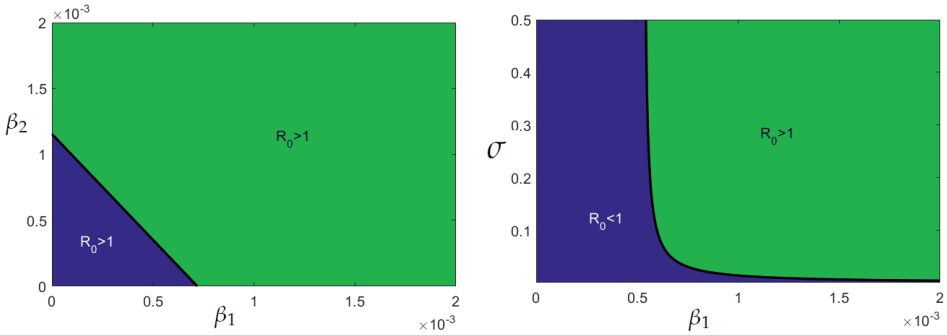

Figure 4. Region of stability of DFE in $\beta_1 - \beta_2$ and $\beta_1 - \theta$ parameter planes. Parameters are the same as in Figure 3.

In Figure 4, we depict parameter regions that characterize the stability properties of the disease-free equilibrium (DFE) and the existence and stability of the endemic equilibrium (EE). The blue-shaded areas correspond to parameter values for which the DFE is locally asymptotically stable, identified by the condition $R_0 < 1$. Conversely, the green-shaded areas indicate regimes with $R_0 > 1$, where the DFE loses stability and a unique endemic equilibrium emerges that is itself stable. The black boundary curves mark the threshold $R_0 = 1$, delineating the transition between disease-free and endemic dynamics. Specifically, Figure 4 (left panel) illustrates stability domains in the (β_1, β_2) parameter plane, while Figure 4 (right panel) presents the corresponding domains in the (β_1, θ) plane. Note that both β_1 and β_2 are scaled by a factor of 10^{-3}.

In the case of $R_0 > 1$, the solution trajectories are demonstrated in Figure 5a–g. The system tends to the endemic steady state E^*. It can be stated that the system converges to the endemic equilibrium point due to the relatively high infection rates. Thus, it becomes clear that Mpox cannot be eradicated without any control measures when the value of the basic reproduction number is higher than one.

The endemic equilibrium is obtained as $S^* = 169.3$, $E^* = 46.86$, $A^* = 25.56$, $I^* = 41.01$, $H^* = 22.78$, $R^* = 742.2$, $M^* = 17.01$. The eigenvalues of the Jacobian matrix are -0.0100, -0.3842, $-0.0301 + i0.0631$, $-0.0301 - i0.0631$, -0.0429, -0.0968, -0.1192, and the condition $|\arg(\rho)| > \frac{\alpha\pi}{2}$ holds for all eigenvalues.

Figure 6 presents numerical trajectories of model (2) under different initial population values. The solutions are displayed in two three-dimensional phase spaces. In the left panel, the trajectories in the (S, E, A)-space illustrate the dynamics of the susceptible population S, exposed population E, and asymptotic population A. Three distinct trajectories, corresponding to different initial conditions, are shown in red, blue, and green. Regardless of the initial states, all trajectories converge to the equilibrium point (S^*, E^*, A^*), highlighted by the black arrow. In the right panel, the trajectories in the (A, I, H)-space describe the evolu-

tion of the asymptomatic population A, infected population I, and hospitalized population H. Similar to the left panel, trajectories arising from different initial conditions converge to the equilibrium point (A^*, I^*, H^*), also indicated by a black arrow. Taken together, these numerical simulations demonstrate that solutions originating from varying initial population values consistently approach the same endemic equilibrium. This convergence provides numerical evidence supporting the global asymptotic stability of the endemic equilibrium for model (2).

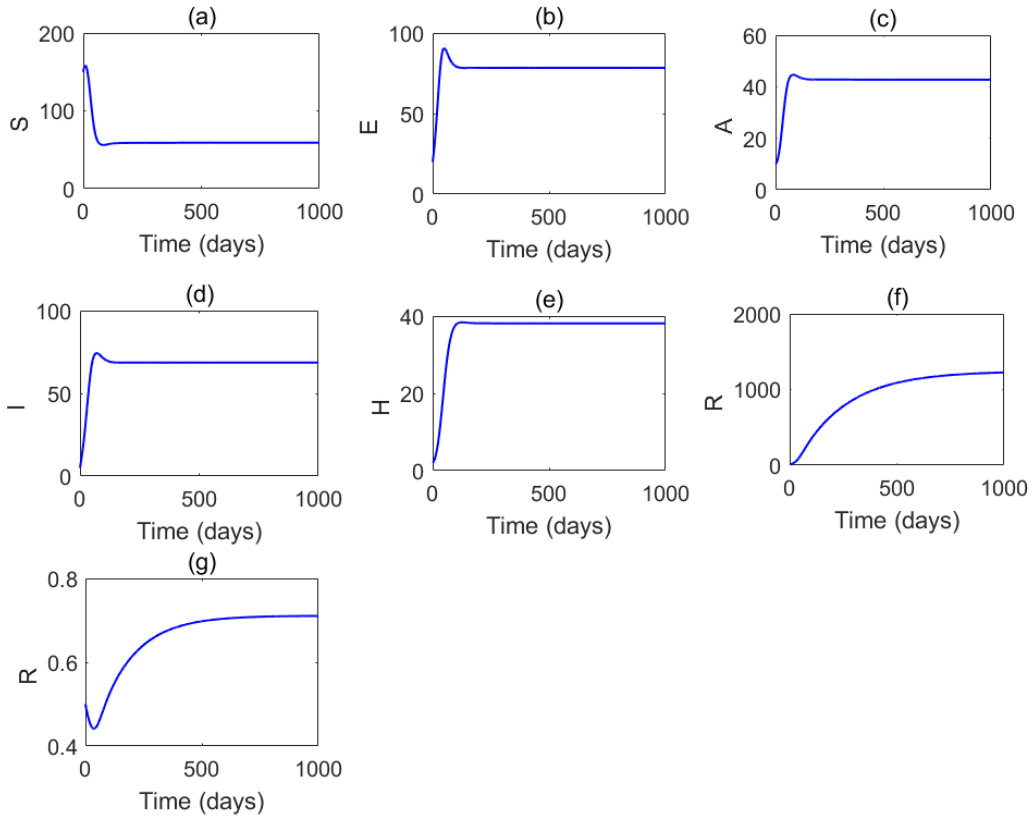

Figure 5. (**a**–**g**) Solutions of system (2) are plotted using parameter values from Table 1 for which $R_0 > 1$.

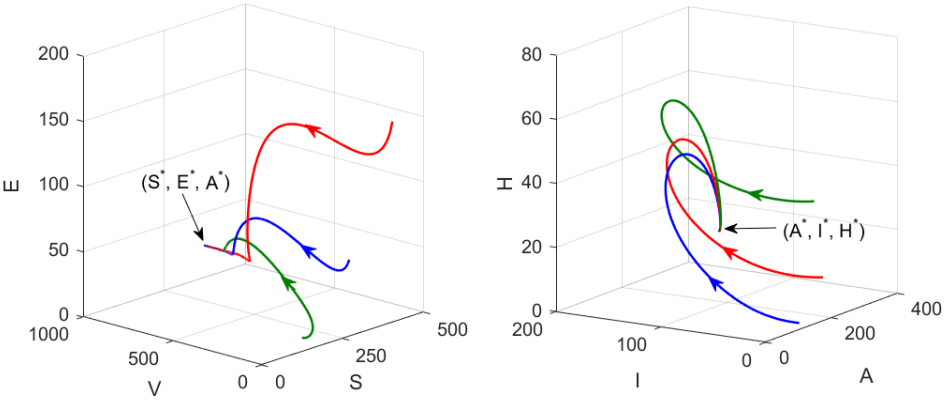

Figure 6. Numerical solutions are plotted for different initial values of model (2) populations. The same set of parameters is used as in Figure 5.

The sensitivity of the dynamics of infection with respect to changes in the value of the fractional order α is depicted in Figure 7. As the value of α moves away from the classical value of $\alpha = 1.0$, decreasing towards a smaller value, the dynamics of the infection exhibit increased flatness and prolongation, a delay in the peak of infection and awareness, and

a slow decay rate. The memory effect of the fractional-order model leads to a prolonged period of time that the infection remains and a reduction in the size of the peak due to smaller values of α. When α takes a value close to 1.0, the system restores the classical infection dynamics profile with quick rising, large peaks, and fast decaying.

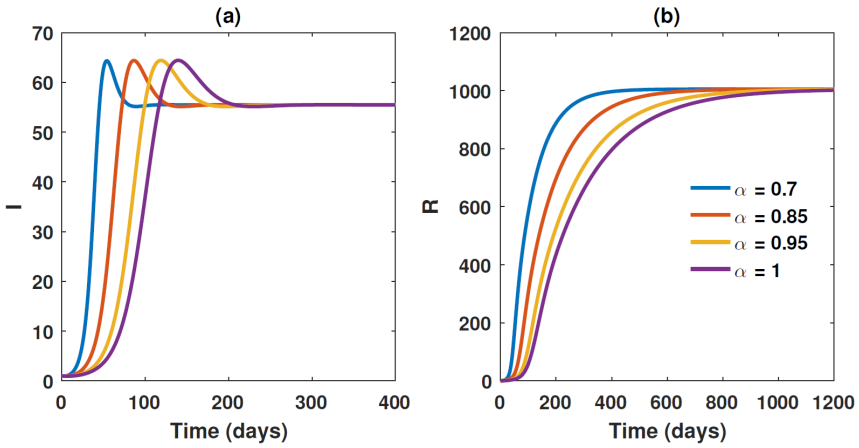

Figure 7. Numerical solutions are plotted for different values of fractional order α. Parameter values are the same as in Figure 5. (**a**) for symptomatic infectious individuals; (**b**) for recovered individuals.

The effect of awareness campaign strategies is presented in Figure 8. In this figure, varying the awareness parameter η within its allowable range results in the dynamics of infection with smaller infected populations, both hospitalization and non-hospitalization types. These results indicate that awareness campaigns are essential for the control of the disease (see Figure 9). Similar dynamics were observed when we varied the awareness activity rate ϕ within its tolerable range. Thus, we can say that awareness campaigns through media are important for minimizing mpox transmission.

Figure 10 depicts the effect of the progression rate θ from the exposed class to the infectious classes. With increasing values of θ from 0.10 to 0.20, S decreases slowly, whereas the decrease in E is relatively more marked. Meanwhile, A, I, H, R, and M all show a monotonous increase with respect to θ. The findings above suggest that a larger value for the progression rate θ means that individuals will quickly move from the exposed class to the various infectious states, resulting in a smaller size of the exposed class at equilibrium and more people being in the infectious, hospitalized, and recovered compartments. The monotonic increase in M is also indicative of an increased mortality burden for faster progression of the infection process. Therefore, it is clear that the progression rate θ is a very important parameter affecting the distribution of people in the various mpox epidemic-related compartments.

Sensitivity Analysis

In order to determine the parameters which have the most impact on the transmission of the disease, the normalized forward sensitivity analysis is conducted for the basic reproductive ratio R_0. The normalized sensitivity index of R_0 to parameter q is defined as

$$\Upsilon_q^{R_0} = \frac{\partial R_0}{\partial q}\frac{q}{R_0}. \tag{63}$$

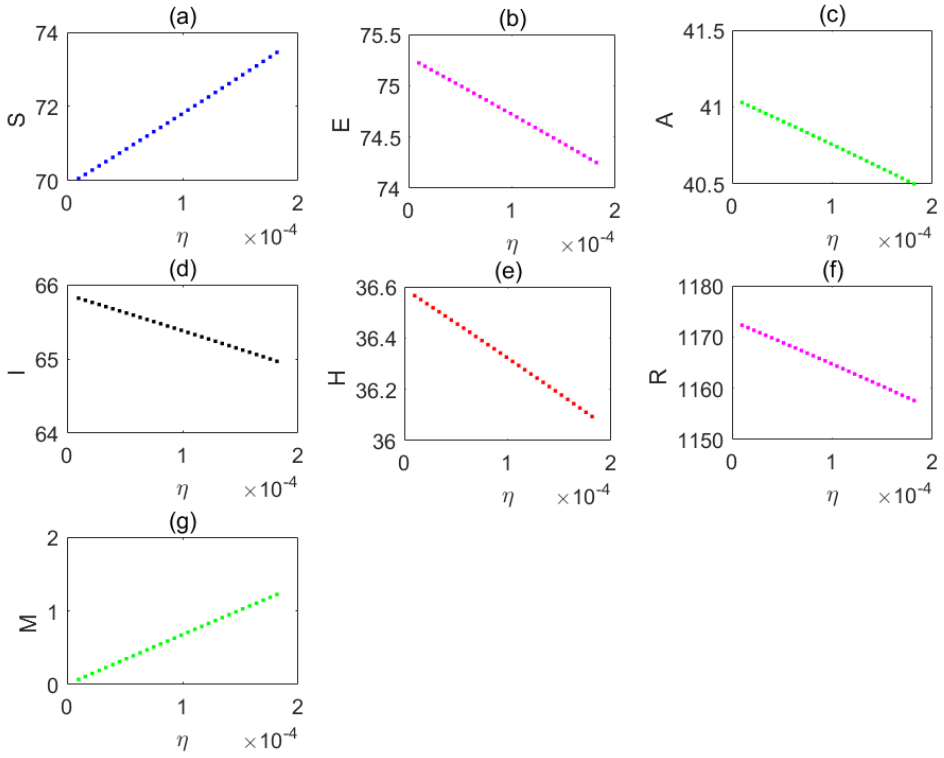

Figure 8. (**a**–**g**) The steady-state solutions are plotted against the rate of organizing awareness campaigns, denoted by η. The remaining parameter values are adopted from Table 1. In generating the figure, the condition given in (1) has been enforced.

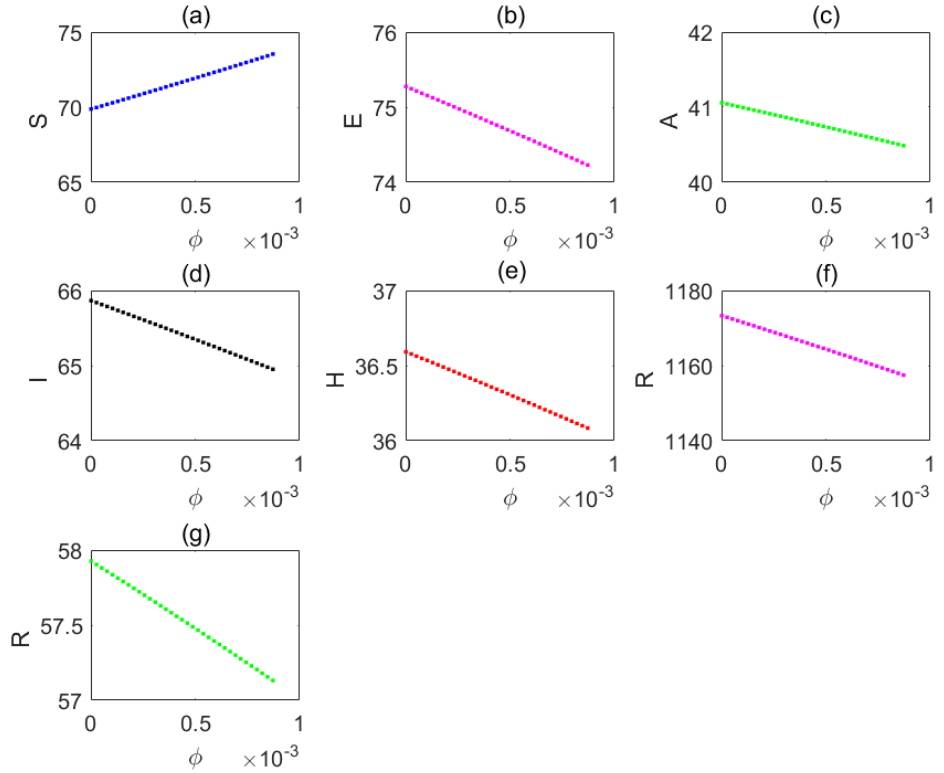

Figure 9. (**a**–**g**) Steady-state values of model population plotted against the rate of the awareness activity rate ϕ. The remaining parameter values are adopted from Table 1. In generating the figure, the condition given in (1) has been enforced.

The basic reproduction number is obtained as

$$R_0 = \frac{\Lambda\theta}{\mu(\theta+\mu)}\left(\frac{p\beta_2}{\gamma_A+\mu}+\frac{(1-p)\beta_1}{\gamma_I+\sigma+\mu+\delta}\right).$$

Using (63), the normalized sensitivity indices are determined as

$$\begin{aligned}
\Upsilon_{\beta_1}^{R_0} &= \frac{(1-p)\beta_1}{(\gamma_I+\sigma+\mu+\delta)Q} > 0,\\
\Upsilon_{\beta_2}^{R_0} &= \frac{p\beta_2}{(\gamma_A+\mu)Q} > 0,\\
\Upsilon_{\Lambda}^{R_0} &= 1, \quad \Upsilon_{\theta}^{R_0} = \frac{\mu}{\theta+\mu} > 0,\\
\Upsilon_{\gamma_A}^{R_0} &= -\frac{p\beta_2\gamma_A}{(\gamma_A+\mu)^2Q} < 0,\\
\Upsilon_{\gamma_I}^{R_0} &= -\frac{(1-p)\beta_1\gamma_I}{(\gamma_I+\sigma+\mu+\delta)^2Q} < 0,\\
\Upsilon_{\sigma}^{R_0} &= -\frac{(1-p)\beta_1\sigma}{(\gamma_I+\sigma+\mu+\delta)^2Q} < 0,\\
\Upsilon_{\delta}^{R_0} &= -\frac{(1-p)\beta_1\delta}{(\gamma_I+\sigma+\mu+\delta)^2Q} < 0.
\end{aligned}$$

where

$$Q = \frac{p\beta_2}{\gamma_A+\mu}+\frac{(1-p)\beta_1}{\gamma_I+\sigma+\mu+\delta}.$$

The values of transmission parameters β_1 and β_2 have a positive impact on R_0, while the values of recovery and removal parameters γ_A, γ_I, σ, and δ have a negative impact on R_0. Therefore, the reduction in transmission or increase in recovery parameters can successfully decrease R_0.

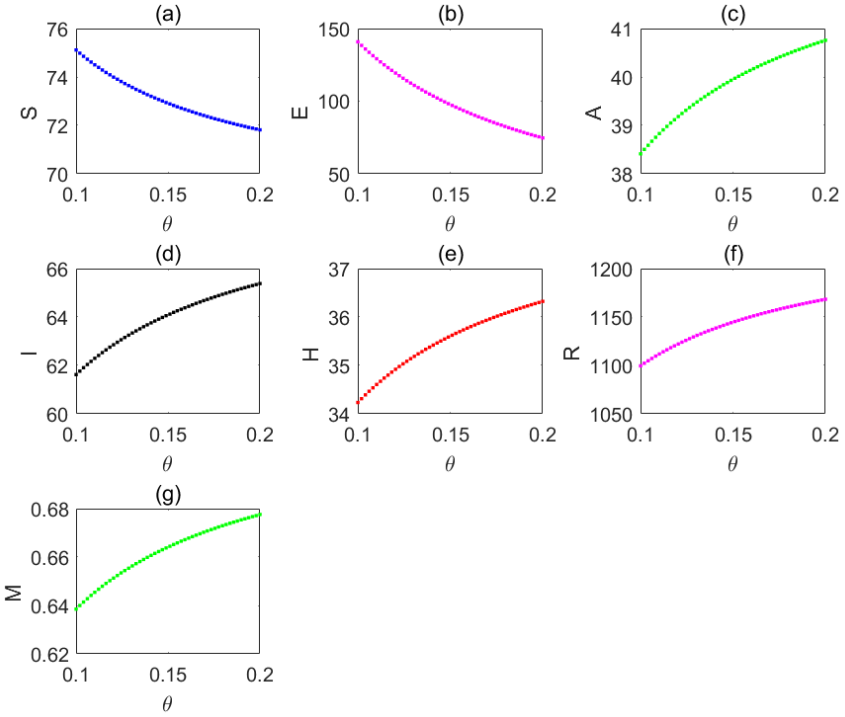

Figure 10. (**a**–**g**) Equilibrium values of the populations plotted versus the progression rate θ from exposed to infectious classes. The remaining parameter values are adopted from Table 1. The condition given in (1) was enforced while plotting this figure.

Normalized sensitivity indices of the model parameters with respect to R_0 are shown in Table 2 and Figure 11. A positive index means an influential parameter in increasing R_0, while a negative index means an influential parameter in decreasing R_0. It is evident from the data that μ has a strong negative effect and Λ has a strong positive effect. Of the transmission parameters, β_1 is more influential on R_0 than β_2. Parameters ϕ, η, ω, γ_H, and δ_H have zero sensitivity as they do not occur in the expression of R_0.

Table 2. Normalized sensitivity indices of model parameters with respect to R_0.

Parameter	Sensitivity Index
β_1	0.681
β_2	0.319
Λ	1.000
θ	0.048
p	0.027
γ_A	-0.289
γ_I	-0.341
σ	-0.213
δ	-0.085
μ	-1.119

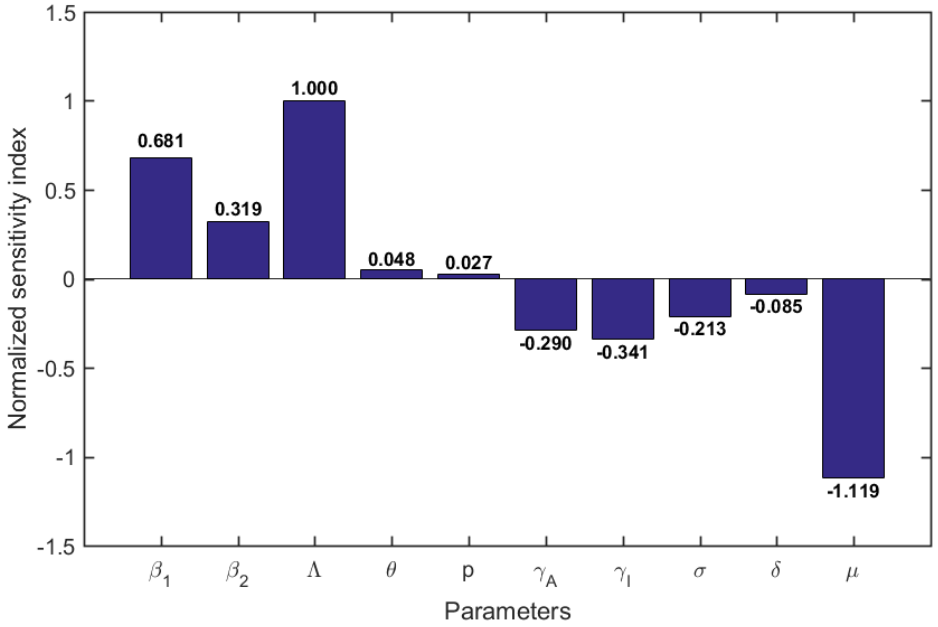

Figure 11. Sensitivity indices of the model parameters using R_0. Parameter values are taken from Table 1.

7. Discussion and Conclusions

In the current study, a mathematical model for mpox virus transmission taking into account public awareness is proposed. This model builds upon the classical model of the epidemic by introducing compartments such as exposed, asymptomatic, infected but not showing symptoms, hospitalized, recovered, and awareness compartments. Furthermore, in the proposed transmission process, the term $(1 - \phi M)$ is taken into account, where the limitation is $\phi \leq \frac{\omega\mu}{\eta\Lambda}$. It must be noted that the Caputo fractional derivative helps incorporate memory into the transmission process of the disease as well as the awareness process. This means that the influence of previous infection and awareness can be incorporated into the model.

From the analysis and numerical simulation, it can be concluded that the basic reproductive number R_0 is very important in deciding the final dynamics of the mpox infection. For the case $R_0 < 1$, the disease-free equilibrium (DFE) is locally asymptotically stable, where the numerically obtained trajectories approach towards the disease-free state. The calculated eigenvalues for the DFE satisfy the fractional-order stability condition $|\arg(\rho)| > \frac{\alpha\pi}{2}$. Therefore, local asymptotic stability of the DFE holds for the chosen set of parameters. From the stability region analysis, it becomes clear that the transmission parameters β_1, β_2, and the progression parameter θ have an effect on the boundary between the disease-free and endemic regimes. Specifically, an increase in the transmission rates decreases the region where $R_0 < 1$.

However, if $R_0 > 1$, the DFE becomes unstable and an endemic equilibrium exists. The numerical simulations show that the solution trajectories tend to the endemic equilibrium $\mathcal{E}^*$. Also, the eigenvalues of the endemic equilibrium meet the condition of fractional-order stability $|\arg(\rho)| > \frac{\alpha\pi}{2}$. Also, the simulations started at different population levels tend to the same endemic equilibrium. This gives numerical justification that the endemic equilibrium is attractive and globally stable. This suggests that mpox will persist in the population if $R_0 > 1$ unless proper control actions are taken. Hence, bringing down the value of R_0 below one becomes important for the elimination of the disease.

The simulation also shows that public awareness-based treatments can be effective control measures, complementing each other. In the case where $R_0 < 1$, the numerical solutions tend to the DFE, which means that if there are appropriate controls applied, the infection can be eliminated. Vaccination helps decrease the number of susceptible people who can get infected with the disease and therefore plays an important role in getting the system into the disease-free region. Moreover, with increases in awareness parameters η and ϕ, the reduction occurs in both the infectious and hospitalized compartments. The analysis of the stable regions together with the simulation provides us with an idea that there is no single measure that could work in any epidemic scenario. If the transmission rate is high enough and $R_0 > 1$, the system tends to an endemic state with the presence of infection. However, awareness-based control measures could help bring down the transmission rate and hence get the system out of the endemic region to the disease-free region by making R_0 less than unity. Moreover, sensitivity analysis of the model parameters using R_0 confirms the main parameters responsible for mpox transmission.

The value of the fractional order α has a significant impact on the time evolution of the epidemic process. The numerical experiments demonstrate that reducing α from its classical value $\alpha = 1$ leads to a smoother and longer epidemic curve, shifts the appearance of peaks of infection and awareness to a later moment, and slows down the reduction in the epidemic variable. This is in agreement with the memory feature of the Caputo derivative, as the present state of the system is influenced by its past states. With α approaching one, the behavior of the epidemic process becomes closer to the classical one, with the rapid rise and fall in the epidemic variables.

Another crucial factor affecting the epidemic model dynamics is the progression rate θ from the exposed class to the different infectious classes. Results from the numerical analysis show that an increase in θ from 0.10 to 0.20 leads to a reduction in the number of exposed individuals and an increase in asymptomatic and symptomatic infectious, hospitalized, recovered, and death classes. It is clear from the result that there is an increased rate of progression from the exposed state to the infectious classes. An increase in the mortality class (M) with θ suggests that quick progression through the infection process can lead to increased mortality.

In conclusion, this study highlights that the fractional-order modeling approach with the impact of awareness captured with the function $(1 - \phi M)$ with restriction (1) gives valuable information regarding the persistence and control of mpox infections. The memory feature embedded in the fractional differential equation can have a significant influence on both the time scale and the peak magnitude of the outbreak, while the reproduction number serves as a threshold between disease elimination and disease persistence. The numerical studies also verify the theoretical analysis of global stability and help reveal the impacts of the fractional order, disease dynamics, and awareness on the epidemic dynamics. Future research needs to be directed toward calibration of the model using mpox outbreak data, estimation of the fractional-order and epidemiological parameters, and the inclusion of a nonlinear awareness and behavioral response function. Furthermore, the present model can be extended to account for periodic vaccination programs, which would lead to the formulation of an impulsive differential equation model [33].

Author Contributions: Conceptualization, I.M.A., and F.A.B.; methodology, I.M.A., and F.A.B.; software, F.A.B., and I.M.A.; formal analysis, F.A.B.; investigation, F.A.B.; writing—original draft preparation, I.M.A., and F.A.B.; writing—review and editing, F.A.B.; visualization, F.A.B., and I.M.A.; supervision, F.A.B.; project administration, I.M.A.; funding acquisition, I.M.A. All authors have read and agreed to the published version of the manuscript.

Funding: This research work was funded by Umm Al-Qura University, Saudi Arabia, under grant number: 26UQU4340243GSSR07.

Data Availability Statement: The original contributions presented in this study are included in the article. Further inquiries can be directed to the authors.

Acknowledgments: The authors extend their appreciation to Umm Al-Qura University, Saudi Arabia for funding this research work through grant number: 26UQU4340243GSSR07.

Conflicts of Interest: The authors declare no conflicts of interest.

References

1. Laurenson-Schafer, H.; Sklenovská, N.; Hoxha, A.; Kerr, S.M.; Ndumbi, P.; Fitzner, J.; Almiron, M.; de Sousa, L.A.; Briand, S.; Cenciarelli, O.; et al. Description of the first global outbreak of mpox: An analysis of global surveillance data. *Lancet Glob. Health* **2023**, *11*, e1012–e1023. [CrossRef] [PubMed]
2. Srivastava, S.; Kumar, S.; Jain, S.; Mohanty, A.; Thapa, N.; Poudel, P.; Bhusal, K.; Al-Qaim, Z.H.; Barboza, J.J.; Padhi, B.K.; et al. The Global Monkeypox (Mpox) outbreak: A comprehensive review. *Vaccines* **2023**, *11*, 1093. [CrossRef] [PubMed]
3. Satapathy, P.; Yoosuf, B.T.; Gaidhane, A.M.; Vadia, N.; Menon, S.V.; Chennakesavulu, K.; Panigrahi, R.; Kaur, M.; Bushi, G.; Favas KT, M.; et al. Mpox: Transmission dynamics, treatment, and innovations. *Ther. Adv. Infect. Dis.* **2025**, *12*, 20499361251357521. [CrossRef] [PubMed]
4. Afzal, M.; Sah, A.K. Effectiveness of Public Health Campaigns on Mpox Awareness and Prevention in Rural India: A Narrative Review. *Infect. Dis. Clin. Pract.* **2025**, *33*, e1450. [CrossRef]
5. Ochieng, F.O. Mathematical modeling of Mpox virus dynamics with a case study of Africa. *Model. Earth Syst. Environ.* **2025**, *11*, 193. [CrossRef]
6. Brand, S.P.; Cavallaro, M.; Cumming, F.; Turner, C.; Florence, I.; Blomquist, P.; Hilton, J.; Guzman-Rincon, L.M.; House, T.; Nokes, D.J.; et al. The role of vaccination and public awareness in forecasts of Mpox incidence in the United Kingdom. *Nat. Commun.* **2023**, *14*, 4100. [CrossRef] [PubMed]
7. Elechi, K.W.; Toluwalashe, S.; Oyelude, A.; Okechukwu, C.I.; Obed, M.; Okoli, G.C.; Alabi, O.J.; Ikechukwu, S.; Offor, O.O.; Adetoye, E.; et al. Building Bridges: The Role of Effective Community Engagement Strategies for Mpox Prevention and Response. *Afro-Egypt. J. Infect. Endem. Dis.* **2025**, *15*, 226–241. [CrossRef]
8. Al Basir, F.; Ray, S.; Venturino, E. Role of media coverage and delay in controlling infectious diseases: A mathematical model. *Appl. Math. Comput.* **2018**, *337*, 372–385. [CrossRef]
9. Sontag, A.; Rogers, T.; Yates, C.A. Misinformation can prevent the suppression of epidemics. *J. R. Soc. Interface* **2022**, *19*, 20210668. [CrossRef] [PubMed]

10. Cruickshank, S.; McKee, M.; Pagel, C. Effective communication and public engagement strategies to counter misinformation about infectious diseases. *Immunol. Cell Biol.* **2026**, *104*, 92–105. [CrossRef] [PubMed]
11. Molla, J.; Sekkak, I.; Ortiz, A.M.; Moyles, I.; Nasri, B. Mathematical modeling of mpox: A scoping review. *One Health* **2023**, *16*, 100540. [CrossRef] [PubMed]
12. Peter, O.J.; Babasola, O.; Ojo, M.M.; Omame, A. A mathematical model for assessing the effectiveness of vaccination in controlling Mpox dynamics and mitigating disease burden in Nigeria and the Democratic Republic of Congo. *J. Appl. Math. Comput.* **2025**, *71*, 5729–5756. [CrossRef]
13. Pesantes-Grados, P.; Escalante-Ccoyllo, N.; Marín-Machuca, O.; Zambrano-Cabanillas, A.W.; Ango-Aguilar, H.; Marín-Sánchez, O.; Chacón, R.D. A compartmental mathematical model to assess the impact of vaccination, isolation, and key epidemiological parameters on mpox control. *Med. Sci.* **2025**, *13*, 226. [CrossRef] [PubMed]
14. Agarwal, R.; Airan, P.; Agarwal, R.P. Exploring the landscape of fractional-order models in epidemiology: A comparative simulation study. *Axioms* **2024**, *13*, 545. [CrossRef]
15. Khan, M.A.; DarAssi, M.H.; Tasqeeruddin, S.; Alzahrani, A.; Jebran, S.; Isa, N.M. A fractional-order vaccination model to analyze the dynamics of Mpox Clade I and II with real data. *Sci. Rep.* **2026**, *16*, 11093. [CrossRef] [PubMed]
16. Petráš, I. *Fractional-Order Nonlinear Systems: Modeling, Analysis and Simulation*; Springer Science & Business Media: Cham, Switzerland, 2011.
17. Shub, M. *Global Stability of Dynamical Systems*; Springer Science & Business Media: Cham, Switzerland, 2013.
18. Nabti, A.; Ghanbari, B. Global stability analysis of a fractional SVEIR epidemic model. *Math. Methods Appl. Sci.* **2021**, *44*, 8577–8597. [CrossRef]
19. Shuai, Z.; van den Driessche, P. Global stability of infectious disease models using Lyapunov functions. *SIAM J. Appl. Math.* **2013**, *73*, 1513–1532. [CrossRef]
20. Pathak, S.; Kota, V.R. Mathematical analysis of an infectious disease model: Stability, persistence, and equilibrium analysis in a non-linear epidemiological system. *J. Nonlinear Math. Phys.* **2025**, *32*, 64. [CrossRef]
21. Naik, P.A. Global dynamics of a fractional-order SIR epidemic model with memory. *Int. J. Biomath.* **2020**, *13*, 2050071. [CrossRef]
22. Kuznetsov, N. Theory of hidden oscillations and stability of control systems. *J. Comput. Syst. Sci. Int.* **2020**, *59*, 647–668. [CrossRef]
23. Lin, Y.C.; Wen, T.H.; Shih, W.L.; Vermund, S.H.; Fang, C.T. Impact of vaccination and high-risk group awareness on the mpox epidemic in the United States, 2022–2023: A modelling study. *eClinicalMedicine* **2024**, *68*, 102407. [CrossRef] [PubMed]
24. Zhang, W.; Zhang, J.; Liu, Q.H.; Zhao, S.; Li, W.Q.; Ma, J.J.; Lu, X.; Boccaletti, S.; Sun, G.Q. Behavior changes influence mpox transmission in the United States, 2022–2023: Insights from homogeneous and heterogeneous models. *PNAS Nexus* **2025**, *4*, pgaf025. [CrossRef] [PubMed]
25. Hidayat, M.A.; Fatmawati; Alfiniyah, C.; Peter, O.J. A Time-Delayed Mathematical Modeling for Monkeypox Transmission with Incubation Period. *Stat. Optim. Inf. Comput.* **2025**, *14*, 3874–3890. [CrossRef]
26. Lei, X.; Meng, X.Y.; Wang, J.G. Stability and bifurcation of Mpox transmission model with population heterogeneity and booster vaccination. *Math. Biosci.* **2026**, *396*, 109659. [CrossRef] [PubMed]
27. Alsulami, I.M. A Fractional Optimal Control Problem for Mpox Integrating Vaccination, Treatment and Awareness Campaign. *Mathematics* **2026**, *14*, 2262. [CrossRef]
28. Greenhalgh, D.; Rana, S.; Samanta, S.; Sardar, T.; Bhattacharya, S.; Chattopadhyay, J. Awareness programs control infectious disease–multiple delay induced mathematical model. *Appl. Math. Comput.* **2015**, *251*, 539–563. [CrossRef]
29. Funk, S.; Gilad, E.; Watkins, C.; Jansen, V.A. Modelling the influence of human behaviour on the spread of infectious diseases: A review. *J. R. Soc. Interface* **2010**, *7*, 1247–1256. [CrossRef] [PubMed]
30. Verma, P.; Kumar, M. Analytical solution with existence and uniqueness conditions of non-linear initial value multi-order fractional differential equations using Caputo derivative. *Eng. Comput.* **2022**, *38*, 661–678. [CrossRef]
31. Castillo-Chavez, C.; Song, B. Dynamical models of tuberculosis and their applications. *Math. Biosci. Eng.* **2004**, *1*, 361–404. [CrossRef] [PubMed]
32. Diethelm, K.; Ford, N.J.; Freed, A.D. A predictor-corrector approach for the numerical solution of fractional differential equations. *Nonlinear Dyn.* **2002**, *29*, 3–22. [CrossRef]
33. Al Basir, F. Dynamics of Infectious Diseases with Periodic Awareness Campaigns. In *Proceedings of the International Workshop of Mathematical Analysis and Applications in Modeling*; Springer: Berlin/Heidelberg, Germany, 2018; pp. 363–370.